Postprint of: “The first crystal structure of human RNase 6 reveals a novel substrate binding and cleavage site arrangement” in *The Biochemical Journal*, v. 473, núm. 11 (Maig 2016), p. 1523-1536. The final version is available at DOI 10.1042/BCJ20160245

Title: The first crystal structure of human RNase 6 reveals a novel substrate binding and cleavage site arrangement.

Authors: Prats-Ejarque[1] G, Arranz-Trullén[1] J; Blanco[1] JA; Pulido[1,2] D; Nogués[1] MV; Moussaoui[1] M; and Boix[1] E¶.

[1] Department of Biochemistry and Molecular Biology, Faculty of Biosciences, Universitat Autònoma de Barcelona, E-08193 Cerdanyola del Vallès, Spain
[2] Present address: Imperial College London, South Kensington Campus London,
London SW7 2AZ, United Kingdom

¶Author to whom correspondence should be addressed; E-Mail Ester.Boix@uab.cat; Tel.: +34-93-581-2565; Fax: +34-93-581-1264

Abstract

Human RNase 6 is a cationic secreted protein that belongs to the RNase A superfamily. Its expression is induced in neutrophils and monocytes upon bacterial infection, suggesting a role in host defence. We present here the crystal structure of RNase 6 obtained at a 1.72 Å resolution, being the first report for the protein three-dimensional structure and thereby setting the basis for functional studies. The structure shows an overall kidney shaped globular fold shared with the other known family members. Three sulphate anions bound to RNase 6 were found, interacting to residues at the main active site (His15, His122 and Gln14) and cationic surface exposed residues (His36, His39, Arg66 and His67). Kinetic characterization, together with prediction of protein –nucleotide complexes by molecular dynamics, was applied to analyse the RNase 6 substrate nitrogenous base and phosphate selectivity. Our results reveal that, although RNase 6 is a moderate catalyst in comparison to the pancreatic RNase type, its structure includes lineage specific features that facilitate its activity towards polymeric nucleotide substrates. In particular, enzyme interactions at the substrate 5' end can provide an endonuclease type cleavage pattern. Interestingly, the RNase 6 crystal structure revealed a novel secondary active site conformed by the His36-His39 dyad that facilitates the polynucleotide substrate catalysis.

Summary statement (40 words)

We describe the first human RNase 6 crystal structure in complex with sulphate anions. Kinetic analysis, site directed mutagenesis and molecular dynamics simulations identified novel substrate recognition and cleavage sites.

Short title: RNase 6 crystal structure and substrate binding sites

Key words: Protein crystallography, RNase k6, RNase A superfamily, sulphate anion, kinetic characterization, molecular dynamics.

Abbreviation list: C>p, cytidine *2',3'*-cyclic phosphate; EDTA, Ethylenediaminetetraacetic acid; GSH, reduced Glutathione; GSSG, oxidized Glutathione; IPTG, Isopropyl β-D-1-thiogalactopyranoside; MALDI-TOF MS, Matrix Assisted Laser Desorption/Ionization Mass spectrometry; MD, molecular dynamics; poly(C), polycytidylic acid; poly(U), polyuridylic acid; poly(A), polyadenylic acid; dsRNA, double stranded RNA; RMSD, root mean -square deviation; Tris, 2-Amino-2-hydroxymethyl-propane-1,3-diol.

INTRODUCTION

The human RNase 6 is a protein belonging to the bovine pancreatic ribonuclease A (RNase A) superfamily, a vertebrate specific family comprising small secretory proteins, sharing a common overall three-dimensional structure and displaying a variety of properties. Together with the first ascribed function of pancreatic RNases to digest RNA, several family members were reported to be involved in innate immunity, showing toxicity against a wide spectrum of pathogens, from virus, bacteria, fungi and protozoa to helminth parasites [1][2][3]. An unusual rapid evolution rate within the family and the antimicrobial properties of distant related members suggested a common ancestral innate immunity role [4][5]. In humans, the family includes eight known members, also called the "canonical RNases" (Figure 1A). Despite their low sequence identity, ranging from 30% to 70%, we observe the conservation of the disulfide bonding pattern and the catalytic triad. All members are highly cationic and are localized at the long arm (q) of human chromosome 14 [6][7].

RNase 6, also named RNase k6, was first identified during a genomic search for a homologous protein of bovine kidney RNase (RNase k2) and localized on q11 region of chromosome 14 [8][9]. The newly identified human mature protein sequence was found to share 72% identity with its bovine RNase k2 counterpart. Divergence of the kidney RNases in comparison to the prototype reference family pancreatic type RNases supported their involvement in a differentiated biological role. Due to the presence of human RNase 6 in a large variety of tissues and its expression in monocytes and neutrophils, it was proposed that it could play a role in host defence. Indeed, recent studies by Becknell and collaborators showed the protein expression in macrophages and epithelial cells at the urinary tract in response to exposure of uropathogenic bacteria [10]. Spencer and co-workers also reported a potent antimicrobial activity *in vitro* against Gram negative and Gram positive bacteria for RNase 6, together with its closest homologue, RNase 7, and proposed both proteins as responsible for the mammalian urinary tract sterility maintenance [11][10]. Experimental evidence was also provided by the reported downregulation of RNase 6 together with other host innate immunity proteins induced by the human immunodeficiency virus (HIV) [12]. RNase 6 displays 55% amino acid identity to RNase 7, and belongs to the RNase 6, 7 and 8 cluster, sharing with them common structural features (Figure 1A). Interestingly, even though it has been found that eosinophil RNase 2 and RNase 3 gene lineages have undergone one of the fastest rates of divergent evolution to produce paralogous genes [13][14], RNase 6 primate gene lineages appear to have evolved in a more conservative mode [9]. On the other hand, a contradictory scenario has been reported in rodents, in which the evolution pace of RNase 6 presents a substantially higher rate [15]. All in all, a similar tendency towards a isoelectric point increase is shared within the eosinophil lineage.

The RNase A superfamily members share a conserved catalytic mechanism that was thoroughly characterized thanks to the pioneering enzymology studies during the first half of the XX's century [16][17][18]. RNase A catalyzes the cleavage of the 3'5' phosphodiester bond of single polynucleotide substrates, showing selectivity for pyrimidines at the main base subsite (B_1) and a preference for purines at the secondary base site (B_2). Degradation of polynucleotide substrate is also assisted by additional binding sites at both sides of the catalytic centre, referred as B_n, R_n and p_n for bases, ribose and phosphate binding respectively [19].

Preliminary kinetic characterization of RNase 6 upon its discovery indicated a moderate catalytic efficiency respect to the family reference member RNase A. Estimation of kinetic parameters using yeast tRNA as a substrate reported about a 40-fold reduced catalytic rate in comparison to RNase 2 [8]. Further side by side comparison of RNase 6 catalytic efficiency confirmed an overall moderate relative catalytic efficiency, higher than RNase 3 but significantly lower than RNase 7 [20][21][22].

In this work we describe the first crystal structure of RNase 6. The protein structural analysis is complemented with its enzymatic characterization to highlight RNase 6 singularity within the RNase A family context.

MATERIALS AND METHODS

Expression and Purification of the Recombinant Proteins

A plasmid containing the gene of recombinant human RNase 6 was transformed in a prokaryote expression system. The cDNA encoding RNase 6 sequence was a kind gift provided by Dr. Helene Rosenberg (National Institute of Health, Bethesda, MD, USA). Mutant variants were constructed using the Quick Change Site-Directed Mutagenesis kit (Stratagene, La Jolla, CA). All constructs were confirmed by DNA sequencing and the purified protein was analyzed by MALDI-TOF MS and N-terminal sequencing.

The genes were subcloned in plasmid pET11c for prokaryote high yield expression. *E. coli* BL21(DE3)-competent cells were transformed with the pET11c/RNase 6 plasmid. The expression protocol was optimized from the previously described procedure [20] to optimize RNase 6 final recovery yield. For high yield expression, bacteria were grown in Terrific broth (TB), containing 400 µg/mL ampicillin. Recombinant protein was expressed after cell induction with 1 mM IPTG added when the culture showed an A_{600} =0.6. The cell pellet was collected after 4 h of culture at 37 °C. Cells were resuspended in 10 mM Tris-HCl, 2 mM EDTA, pH 8, and sonicated at 50 watts for 10 min with 30-s cycles. After centrifugation at 15,000 x g for 30 min, the pellet fraction containing inclusion bodies was processed as follows: the pellet fraction was washed with 50 mM Tris-HCl, 2 mM EDTA, 0.3 M NaCl, pH 8, and after centrifugation at 20,000 x g for 30 min, the pellet was dissolved in 12 ml of 6 M guanidine HCl, 0.1 M Tris-acetate, 2 mM EDTA, pH 8.5, containing 80 mM GSH, and incubated under nitrogen for 2 h at room temperature. The protein was then refolded by a rapid 100-fold dilution into 0.1 M Tris-HCl, pH 7.5, containing 0.5 M L-arginine, and GSSG was added to obtain a GSH/GSSG ratio of 4. Dilution in the refolding buffer was adjusted to obtain a final protein concentration of 30–150 µg/mL. The protein was incubated in refolding buffer for 48–72 h at 4 °C. The folded protein was then concentrated, buffer exchanged against 0.015 M Tris-HCl, pH 7, and purified by cation exchange chromatography on a Resource S column equilibrated with the same buffer. The protein was eluted with a linear NaCl gradient from 0 to 2 M in 0.015 M Tris-HCl, pH 7 buffer. Further purification was achieved by a reverse phase chromatography on a Vydac C4 column, using the same buffers as described for the Resource S chromatography. The homogeneity of the purified proteins was checked by 15% SDS-PAGE and Coomassie Blue staining and by N-terminal sequencing. RNase 3 and RNase 7 were expressed as previously described [23][24].

Spectrophotometric Kinetic Analysis

Poly(C), Poly(U), Poly(A):Poly(U), CpA, UpA, UpG and C>p (Sigma, Aldrich) were used as substrates, and the kinetic parameters were determined by a spectrophotometric method as described [20]. RNase A, used as a control protein, was purchased from Sigma. Assays were carried out in 50 mM sodium acetate, 1mM EDTA, pH 5.5, at 25 ºC, using 1-cm path length cells. Substrate concentration was determined spectrophotometrically using the following extinction coefficients: ε_{268}= 8400 M^{-1} cm^{-1} for C>p; ε_{265}= 21000 M^{-1} cm^{-1} for CpA, ε_{261}= 23500 M^{-1} cm^{-1} for UpA, ε_{261}= 20600 M^{-1} cm^{-1} for UpG, ε_{268}= 6200 M^{-1} cm^{-1} for poly(C); ε_{260}= 9430 M^{-1} cm^{-1} for poly(U) and ε_{260}= 4430 M^{-1} cm^{-1} for poly(A):poly(U) for each nucleotide unit. The activity was measured by following the initial reaction velocities using the difference molar absorbance coefficients, in relation to cleaved phosphodiester bonds: $\otimes\varepsilon_{286}$= 1450 M^{-1} cm^{-1} for CpA, $\otimes\varepsilon_{286}$= 570 M^{-1} cm^{-1} for UpA, $\otimes\varepsilon_{280}$= 480 M^{-1} cm^{-1} for UpG, $\otimes\varepsilon_{250}$= 2380 M^{-1} cm^{-1} for poly(C), $\otimes\varepsilon_{282}$= 829 M^{-1} cm^{-1} for poly(U) and $\otimes\varepsilon_{260}$= 3400 M^{-1} cm^{-1} for poly(A):poly(U) for

transphosphorylation reaction, and $\otimes\varepsilon_{286}$= 1450 M^{-1} cm^{-1} for C>p hydrolysis reaction [20][25]. Duplicates of seven substrate concentrations (ranging from 0.1 to 2 mM) were tested for each condition. Final enzyme concentrations were selected from 0.1 to 10 µM depending on the RNase activity for each assayed substrate. Kinetic parameters were obtained by the nonlinear regression *GraFit* data analysis program (Erithacus Software). Relative activity of RNase mutants was calculated by comparison of initial velocities (V_0), using a substrate concentration of 0.1 mM for dinucleotides and 0.5 mg/mL for polynucleotides.

Activity staining gel

Zymograms were performed following the method previously described [26]. 15% polyacrylamide-SDS gels were cast with 0.3 mg/mL of poly(C) (Sigma, Aldrich) and run at a constant current of 40 mA for 1.5 h. Following, the SDS was extracted from the gel with 10 mm Tris/HCl, pH 8, and 10% (v/v) isopropanol. The gel was then incubated in the activity buffer (0.1 m Tris/HCl, pH 8) to allow enzymatic digestion of the embedded substrate and then stained with 0.2% (w/v) toluidine blue (Merck, Darmstadt, Germany) in 10 mm Tris/HCl, pH 8, for 10 min. Positive bands appeared white against the blue background. The loading buffer had no 2-mercaptoethanol to facilitate recovery of active enzymes. RNase A (Sigma, Aldrich) was used as a control.

Analysis of polynucleotide cleavage pattern

The characterization of the RNases substrate cleavage pattern was carried out by studying the digestion product profiles, as previously described [27]. The poly(C) substrate (Sigma, Aldrich) was dissolved at a concentration of 0.5 mg/mL in 10 mM HEPES-KOH at pH 7.5. Following, 50 µl of the poly(C) solution were digested with 10 µl of enzyme solution at 25°C during 1 h. Enzyme final concentrations were adjusted for each RNase: 50 nM for RNase 6 and RNase 6-H36R and 1.4 µM for RNase 6-H15A and RNase 7-H15A. At different digestion times the products of the reaction were separated by reversed-phase HPLC column (Nova Pak C18, Waters) according to the previously described procedure [27][28]. Briefly, the RNase- poly(C) reaction mixtures (50 µl and 15 µl for wild-type and mutant RNase 6 respectively) were injected into the column equilibrated with solvent A (10% (w/v) ammonium acetate and 1% (v/v) acetonitrile) and the elution was carried out by an initial 10-min wash and 50-min gradient from 100% solvent A to 10% solvent A plus 90% solvent B (10% (w/v) ammonium acetate and 11% (v/v) acetonitrile). Product elution was detected from the absorbance at 260 nm, and peak identification was performed according to previous characterization of oligocytidylic acids[29].

Protein crystallization

RNase 6 crystals were obtained after high through screening of available commercial kits by the hanging drop vapour diffusion methodology at 20ºC. In one of these kits, *JCSG-plus™ HT-96* (Molecular Dimensions), RNase 6 at 10 mg/mL was able to crystallize under one condition (0.2 M NaCl; 0.1 M Na cacodylate; 2 M $(NH_4)_2SO_4$; pH 6.5). This condition was optimized to improve the crystal size by the hanging drop methodology by mixing 1 µL of the protein sample with 1 µL of the crystallization buffer. The best condition resulting from this optimization was: 0.05 M NaCl, 0.1 M Na Cacodylate (pH 6.5) and 2 M NH_4SO_4. Cubic shaped crystals appeared after 10 days of incubation at 20 °C and were soaked in the cryoprotectant solution by adding 15 % glycerol to the crystallization buffer prior to X-ray exposure.

Data collection, processing and protein structure solving

Data were collected at the XALOC BL13 beamline station of ALBA synchrotron (Spain) using a λ = 0.9795 Å. Data collection was performed at 100ºK using *a Pilatus* 6M detector *(Dectris®,* Switzerland), 800 images were taken at t_{exp} = 0.2 s, $\Delta\varphi$ = 0.2°.The data obtained was processed with *XDS* (MPI for Medical Research, Heidelberg) [30].

Structure was solved by molecular replacement with Phenix Phaser-MR program using an RNase 6 model constructed upon NMR structure of RNase 7 (PDB ID:2HKY) [31]. Iterative cycles of refinement and manual building were applied using *PHENIX* [32] and *Coot* [33] respectively until no further improvement of R_{free} could be achieved. Finally, the stereochemistry of the structure was validated with *SFCHECK* [34] and *WHAT_CHECK* [35]. Table 1 shows all the data collection and structure refinement statistics.

Structure modelling

Molecular modelling predictions were carried out using protein -nucleotide docking and molecular dynamics (MD) simulations. Docking simulations were conducted with *AutoDock 4.2.6* (Scripps Research Institute. La Jolla, CA) and MD simulations were performed with GROMACS 4.5.5 [36]. RNase A and RNase 6 complexes with dinucleotides (CpA, UpA and UpG) were predicted. The initial RNase A- dinucleotides' positions were determined in basis of crystallographic data of RNase A bound to d(CpA) [37]. For RNase 6 -dinucleotide complexes the position of the S1 sulphate was taken as reference. Due to the inactive position of His122 in the RNase 6 crystal, the position of the histidine was adjusted to the "active" conformation taking RNase A as a reference (PDB ID: 1RPG).

For MD simulations the force field AMBER99SB-ILDN [38] was used both for protein and RNA components. All the complexes were centred in a cubic cell with a minimum distance box-solute of 1.0 nm. The unit cell was filled with transferable intermolecular potential 3P (TIP3P) water [39] in neutral conditions with 150 mM of NaCl. Neighbour search was performed using a group cut-off scheme with a cut-off of 1.4 nm for van der Waals interactions and 0.9 nm for the other short-range Lennard-Jones interactions. For long range interactions, smooth particle mesh of Ewald (PME) [40,41] was used with a fourth-order interpolation scheme and 0.16-nm grid spacing for FFT. The bonds were constrained with the P-LINCS algorithm [42], with an integration time step of 2 fs. The energy of the system was minimised using the steepest descendant algorithm and equilibrated in two steps. First, an initial constant volume equilibration (NVT) of 100 ps was performed with a temperature of 300 K using a modified Berendsen thermostat. Then, 100 ps of constant pressure equilibration (NPT) was run at 1 bar with a Parrinello-Rahman barostat [43,44] at 300 K and the same thermostat. Finally, 20 ns production runs were performed under an NPT ensemble without applying restraints. Three independent simulations in periodic boundary conditions were conducted for each complex. The evolution of the average RMSD for all non hydrogen ligand atoms after least square fitting to the original position was calculated.

For prediction of the RNase 6-heptanucleotide complex, the RNase A- d(ATAA) crystal structure was taken as a reference (PDB ID:1RCN; [45]). First, the d(ATAA) coordinates were used to build an AUAA ribonucleotide. His122 of RNase 6 was fixed in the corresponding active conformation. Local search docking with 2000 cycles and 2000 iterations was performed with *AutoDock* 4.2.6 [46] to adjust the AUAA position to RNase 6 active site. Then, three cytidines were added to the 5' end of the tetranucleotide. The sulphate positions of the RNase 6 structures were taken as a reference to place the phosphates corresponding to the extended nucleotide. Following, a steepest descent energy minimization of the complex was performed with *GROMACS* 4.5.5. Molecular dynamics simulations were also applied using the same protocol described for dinucleotides.

Prediction of pK_a values

Prediction of pK_a values of selected protein residues was performed using the Rosetta online server *ROSIE* [47]. The estimated pK_a values of selected His residues were calculated by using a neighbour sphere of 15 Å and considering the protonation state of ionisable residues. A starting pK_a reference value of 6.3 for each His was ascribed. The program evaluates all potential conformational rotamers together with the influence

of side chain and backbone mobility. RNase A (PDB ID: 7RSA) coordinates were used as a reference control. Predicted pK_a values for His12, His105 and His119 residues in RNase A were found in accordance with the previously reported experimental values [48]. His105 in RNase A and His67 in RNase 6 were selected as control solvent exposed residues, not involved in Coulombic interactions with nearby residues. The RNase A double mutant (RNase A-H7H10) [49] crystal structure (PD ID: 5ET4; Blanco et al., unpublished results) was also analysed to evaluate the predicted pK_a values for an engineered secondary site located at RNase A secondary phosphate binding site.

RESULTS

RNase 6 three-dimensional structure

RNase 6 crystals diffracted to 1.72 Å. The structure was solved using RNase 7 structure as a model (PDB ID: 2HKY; [31]). The crystallographic statistics for the data collection, processing and structure solving are provided in Table 1. Structural data for RNase 6 structure is available at the *Protein Data Bank* under the accession number PDB ID:4X09.The RNase 6 three-dimensional structure (Figure 1B) complies the RNase A superfamily overall conformation, with a kidney shaped structure formed by 7 β-strands and 3 α-helices cross-linked by four conserved disulphide bonds, as listed in Table S1. Loop residues Trp1-Lys3, Gln17-Leu21, Lys63-Arg66, Gly86-Gln90 and Pro108-Ser112 are partially disordered. In particular, practically no electron density was visualised for residues Pro2, Lys3, Gln17, Leu21, Gly86 and Lys87, that could not be not properly modelled. Alternate side chain conformations were modelled for some residues (Gln14, Asn32, Ser59, His67, Met78 and Thr79). Specifically, high motion values were observed in loops L1, L2 and L8, where 4% of the residues are disordered, as reported for RNase 7 structure [31].Residues involved in crystal packing were analysed by the *PISA* web server [50]. The intermolecular contacts are listed in Table S2. Interactions are found mostly between β3, β4, β5 and β7 strand residues (Gln71, Arg82, Ala97-Tyr99, Ser125, Ile126) and loop residues. No packing contacts are seen in the environment of the active site, therefore enabling further substrate binding studies.

An overall comparison of RNase 6 crystal structure with previously solved structures of RNase A superfamily members highlighted some interesting particularities. First of all, we observed a distinct conformation of the RNase 6 N-terminus, where Trp1, unique in the RNase A superfamily, folds back towards the protein core. Following, we found several non conserved His residues, unique for RNase 6, that contribute to the protein structure peculiarities. His 9 was observed to interact with Glu12 by a salt bridge, which would participate in the stabilization of the first alpha helix, as reported in RNase A for the Glu2-Arg10 salt bridge [51][52]. Unusual rotamer conformations, showing an unambiguous electron density, were observed for two non conserved histidines: His36 and His 67.

RNase 6 sulphate binding sites

The protein was crystallized in the presence of ammonium sulphate and four sulphate anions were identified in the crystal asymmetric unit (Figures 1B and S1). Three of these sulphates corresponded to defined cationic regions exposed at the protein surface and correlate to putative RNA phosphate binding sites, while the fourth sulphate is involved in the crystal packing. Sulphate anion interactions with nearby residues are listed in Table S3 and illustrated in Figure 2. Sulphate labelled as S1 corresponds to the active site of the enzyme, conserved in all canonical RNases. The presence of either a sulphate or phosphate anion at the enzyme active site was already reported for RNase A [53][54] and other family members: RNase 2/EDN [55], RNase 3/ECP [56] and RNase 5/angiogenin [57]. On the other hand, the second sulphate (S2)

found in RNase 6 structure binds to a distinct region not reported in any other family members (Arg66/His67). Comparative studies of our structure with the RNase A-tetranucleotide analogue [45] suggested that this region may represent a distinct phosphate interaction subsite located at the 5' end of the RNA substrate. Following, a third sulphate anion was visualized in RNase 6 structure bound to two His residues (His 36 and His 39), His 39 being unique for RNase 6 among all the RNase A members. Interestingly, both His residues together with a close by Lys (Lys87) mimic the disposition of a putative RNase active site (Figure 3), as also identified using the *PDBeMotif* analysis tool available at the PDBe server (http://www.ebi.ac.uk/pdbe-site/pdbemotif/).

RNase 6 main active site

The RNase 6 crystal structure illustrated the conservation of the active site architecture within the RNase A family. Residues His15, Lys38 and His122 (His12, Lys41 and His119 RNase A counterparts) build the active site groove, with His122 adopting the so-called *inactive* orientation [58], a conformation reported to be favoured in acidic and high ionic salt solutions [59]. Comparison of atomic crystal structures for RNase A indicated that His119 can adopt two conformations: A (active) and B (inactive), where the *active* ring orientation is required for adenine binding at the secondary base B_2 site [37][60]. On the other hand, the *active* orientation of RNase A His119 ring was reported to be favoured by the hydrogen bond interaction with the vicinal Asp121 residue, whose interaction would account for the correct His119 tautomer in catalysis [61]. RNase 6 counterpart (Asp124), located in an equivalent conformation, could also perform an equivalent role. However, inactive His122 conformation is fixed in our RNase 6 structure by an hydrogen bond interaction with Lys7. Therefore, proximity of Lys7 might alter significantly the properties of the His122 catalytic residue. Likewise, we considered the potential influence of the nearby His 36/His 39 RNase 6 residues on the other active site His (His15). The presence of cationic residues nearby to RNase 6 active site could shape the enzyme performance, and may account for a reduction of its catalytic efficiency in comparison to RNase A (Table 2, Table S4). Although RNase 6 structure conserves equivalent positions for some key residues at the active site environment, as Gln14 and Asn41 (Gln11 and Asn44 respectively in RNase A), the proximity of residues such as Lys7, His36 or His39 should not be disregarded.

RNase 6 nucleotide binding sites

Following, RNase 6 crystal structure was further analysed to elucidate the structural basis for the protein substrate specificity and kinetic properties. Comparison of RNase 6 structure with RNase A indicated conservation of most residues at the B_1 site. In contrast, non conserved substitutions were found for Phe120 and Ser123 RNase A counterpart residues. Phe120 is observed in RNase A to contribute by stacking interactions to fix the pyrimidine ring [37]. Nevertheless, a Leu residue in RNase 6, also presents in RNase 3, might also contribute to shape the protein base binding hydrophobic cavity. In any case, the presence of Phe120 in both RNase A and RNase 4, two very efficient RNase A family members, might also explain their relative higher catalytic activity. On the other hand, B_1 selectivity is considered dependant on a Thr–Asp dyad relative position. Thr45-Asp83 interactions were attributed in RNase A to shift from cytidine to uridine preference [17]. However, in RNase 6 the presence of Gln 40, hydrogen bonded to Asp 80 (Asp83 counterpart), is fixing the later in a distinct orientation, that might interfere in its interaction with Thr42 (Thr45 counterpart), and modifies the pyrimidine binding mode. Additionally, RNase A and RNase 4 (an RNase with an unusual strong uridine preference [62]), have an hydrophobic residue at Gln40 position, which was considered to help locating the Thr45 residue at the most favoured conformation for uridine base binding [63]. To note, Gln40-Asp80 pair is unique to RNase 6 among the 8 human canonical RNases (Figure 1). This scenario might explain in RNase 6 the observed increase K_m value for both UpA and CpA respect to

RNase A (Table 2). On the other hand, the orientation of Asp80, closer to RNase A counterpart but clearly distinct from RNase 4, may explain RNase 6 moderate preference for uridine at B_1 site (Table 3). Interestingly, uridine predilection of RNase 4 would be mostly determined by Arg101 residue that can directly interact with the uridine carbonyl group and is bringing the Asp80 closer to the Thr45 vicinity [64]. Noteworthy, the presence of Arg101 is characteristic of the RNase 4 lineage, whereas RNase A and RNase 6 have a Lys at this position which is pointing to the opposite direction.
Next, we analysed RNase 6 structure at the secondary base site (B_2). Conservation of Asn68 and Asn64 (Asn71 and Asn67 in RNase A respectively) is observed. Notwithstanding, the presence of a non conserved cationic residue at position 66 might alter significantly the region. Additionally, although there is a conservative substitution for Glu111 in RNase A (Asp107 in RNase 6), the distinct loop orientation, due to the presence of a Pro in RNase 6, modifies considerably the region putative interactions. Altogether, the B_2 site architecture would provide reduced binding interactions to the purine base, retaining a preference for adenine versus guanine, as confirmed by our kinetic results (Tables 2, 3 and S4) and reported for most of the other tested mammalian RNase A family members [65][66][67]. Finally, we searched the RNase 6 structure for phosphate binding sites that could contribute to the recognition of an RNA polymeric substrate, as described for RNase A [19]. Towards this aim, the protein nucleotide binding mode was further analysed by molecular modelling.

Structure analysis by molecular modelling simulations
Molecular dynamics simulations were performed to predict the overall RNase 6 substrate binding mode. Three independent runs were carried out for a total of 20 ns. All ligand positions were fully stabilized after a time lapse of 5 ns, showing a final average RMSD ranging from 0.15 to 0.3 nm. First of all, molecular dynamics simulations were applied to RNase dinucleotide complexes taking as a model reference the RNase A-d(CpA) crystal structure[37]. Results indicated that the CpA and UpA dinucleotides could accommodate in a similar orientation into the RNase 6 catalytic cleft, showing no significant displacement from the original location (Figure 4). A close by inspection of predicted RNase 6 -dinucleotide interactions corroborated some of the structural features inferred from the crystal structure analysis. Equivalent interactions at the phosphate position suggested a conserved binding mode at the main phosphate binding site (p_1). Noteworthy, although the starting position of His122 in RNase 6 crystal was found in the inactive conformation, the residue was adjusted to its active orientation before modelling, remaining in favoured orientation for catalysis after all MD simulations. Interestingly, together with equivalent relative positioning of Gln14, His15 and His122, the presence in the RNase 6 active site neighbourhood of Lys7 and Trp10 residues (Ala4 and Lys7 in RNase A) would account for significant differences at the p_1 environment.
The binding pattern described for RNase A was also mostly conserved for RNase 6 at the main pyrimidine base site (B_1). Leu123 in RNase 6 was observed to partially supply the Phe120 stabilizing role in RNase A, but might induce a minor tilt of the ring plane. Interestingly, together with the conserved bidentate hydrogen bond between Thr42 and the pyrimidine base, the close by Gln40 could directly interact with the Asp80 and the N3 atom of the pyrimidine base.
On the other hand, the comparison between the secondary base binding site (B_2) of both RNases showed minor differences in the relative position of the adenine base, but a more pronounced base displacement for the guanine containing dinucleotides. Equivalent hydrogen bond interactions to adenine were found in RNase 6 for Asn64 and Asn68 (Asn67 and Asn71 in RNase A), together with base stacking interactions with His122 (His119 in RNase A). However, although the main determinants for adenine binding were conserved, we observed how the presence of Arg66, unique for RNase 6, is significantly altering the environment. Indeed, in all our predicted protein-dinucleotide complexes we observed a salt bridge between Arg66 and Asp107, which

shifted the Asp position from the corresponding RNase A anionic residue (Glu111).
In particular, a major displacement from the original position was observed for the UpG dinucleotide in complex with both RNases. Molecular dynamics simulations indicated that the guanine base could not properly fit into the B_2 site, promoting non canonical orientations, where the guanine base was partially displaced. Moreover, in both RNases, the bidentate hydrogen bond by Asn68 (Asn71 in RNase A) was partially lost. Variability among replicates in the dinucleotide positioning reminded the reported productive and non productive binding mode for the crystallographic complexes of RNase A with 2'5'-UpG [68]. Additionally, interactions in both RNases between the guanine C2 amino group and the Asp107 (Glu111 in RNase A) residue would fix the base in a less favoured orientation, pushing away the phosphate from the main active site. Nonetheless, the relative UpG displacement from the original position was less pronounced in the predicted RNase A complex, probably due to the contribution of Phe120 stacking interactions at B_1, that provide a better fixation of the pyrimidine base. On its side, the presence in RNase 6 of Lys7 close to the active site environment would favour the displacement of the phosphate towards the p_2 region.

Complementarily, to gain further insight into the protein nucleotide binding mode we modelled an -heptanucleotide complex taking the RNase A-d(ApTpApA) crystal structure [45] as a starting reference model (Figure 5). The oligonucleotide fitted nicely into the enzyme active cleft showing only significant differences from the RNase A binding mode at the secondary substrate binding sites. Figure 5 highlights the protein residues at hydrogen bond distance observed in the protein –heptanucleotide complex. Putative RNase 6 substrate binding sites were ascribed for base and phosphate recognition (Table S5). Together with conserved equivalent sites to RNase A, the predicted complex illustrated the presence in RNase 6 structure of unique interacting residues at the RNA 5' end. A novel specific region at p_{-2} and p_{-3} sites would be conformed by residues His36, His39, Lys87. Besides, stacking interactions between His36 and the base located at B_{-2} position were also identified in the model.

Kinetic characterization of RNase 6
Next, we determined the RNase 6 enzymatic activity against a variety of RNA substrates to correlate the protein structure with its enzymatic properties. RNase 6 catalytic efficiency ratio was compared with RNase 3 and RNase A (Table S4), as representative family members for low and high catalytic efficiency respectively [66][18][23].
First, kinetic parameters for RNase 6 were calculated for dinucleotide and cyclic mononucleotide substrates (Table 2). Comparison of K_m and k_{cat} values for cyclic mono and dinucleotides indicated that most of the decrease of the catalytic efficiency of RNase 6 in comparison to RNase A (from 100 to 1000 fold) is due to a reduction in the catalytic constant value. A side by side comparison of substrate relative ratio (Table 3) highlighted for RNase 6 a preference for uridine at B_1 site and selectivity for adenine at B_2. Additionally, the enzyme activity was assayed against polymeric substrates (Tables 3 and S4). RNase 6 displayed a low catalytic efficiency for polynucleotides in comparison to RNase A (Figure S2), showing a similar reduced relative catalytic activity as previously reported for RNase 3 [20]. Interestingly, we observed that RNase 6 had the ability to degrade the double stranded poly(U):poly(A) substrate, a property not shared by RNase 3.
Complementarily, to evaluate the contribution of RNase 6 specific subsite arrangement, we analysed the enzyme poly(C) cleavage pattern, as model of polymeric substrate (Figure 6). The oligonucleotides obtained from the substrate digestion were eluted by reversed-phase chromatography, where the mononucleotide fraction is eluted at the initial conditions and oligonucleotides of increasing size elute at increasing retention times. The previously optimized methodology distinguishes between consecutive sizes up to 8 or 9 nucleotides, whereas the peaks corresponding to higher molecular mass

components contain more than one oligonucletide size due to the column discrimination power limitations [29]. Our previous work on RNase A cleavage pattern showed a decrease of the initial poly(C) peak followed by the formation of intermediate oligonucleotides with an average size around 6–7 residues, a pattern that supported the enzyme multisubsite structure providing a characteristic endonuclease type activity [29]. Noteworthy, RNase 6 displayed a characteristic digestion profile differentiated from that previously obtained for RNase A [27], where there is first the formation of considerably large intermediates which are subsequently digested, giving rise to relatively shorter intermediates. Interestingly, the decrease of the original polynucleotide substrate was enhanced for RNase 6 at short incubation times. On the other hand, the predominance of smaller oligonucleotides did not take place until most of the high molecular mass polymeric substrate has been degraded, revealing a singularized cleavage pattern, that could be ascribed to a pronounced endonuclease mechanism.

Kinetic characterization of RNase 6 mutants

Analysis of RNase 6 three dimensional structure and molecular modelling predictions suggested that the enzyme facility to cleave polymeric substrates could be related to the presence of surface exposed cationic residues that might facilitate the RNA anchorage and degradation. Noteworthy, the presence in RNase 6 of a His pair (His 36/His39) (Figures 1 and S3) that adopts a configuration equivalent to the His15/His122 dyad at the RNase main active site, suggested the existence of a secondary active centre (Figure 3). To evaluate this hypothesis we designed mutant variants at His15 and His36. First, the enzyme main active site was removed by His15 mutation to alanine. Residue His15 in RNase 6 was selected as RNase A His12 counterpart, where the corresponding H12A mutant was reported by Raines and co-workers to totally abolish the RNase A catalytic activity [69]. Additionally, His36 was mutated to Arg to remove the putative secondary catalytic His while retaining an exposed cationic charge. Besides, most RNase A family members, including RNase 7, the closest RNase 6 homologue, display an Arg at an equivalent position (Figures 1 and S3). Eventually, a double mutant (His15A/His36A) was engineered to evaluate simultaneously the removal of the main and secondary active sites.

Kinetic characterization of point mutants confirmed the key role of both His15 and His36 (Table 4). Contribution of His36 was found mostly critical for polymeric substrates. On the other hand, we observed how the RNase 6 His15 to Ala mutant was retaining a significantly high activity for polymeric substrates (about 35-40% relative activity respect to wild-type RNase). Interestingly, for the assayed dinucleotides, a residual relative activity of about 15% was observed, which was abolished by the double mutation. Moreover, the RNase 6-H15A activity was further compared with the corresponding RNase 7-H15A mutant (Table 4). The complete abolishment of activity for the RNase 7 active site mutant for dinucleotides, in contrast to RNase 6-H15A, corroborated the hypothesis. On the other hand, a remnant activity for polynucleotides is observed for both the RNase 6 double mutant and RNase 7-H15A mutant. Likewise, residual catalytic activity for the RNase A-H12K/H119Q mutant was attributed to be solely promoted by the RNA structure distortion induced by the enzyme interaction[49]. Complementarily, the analysis of RNase 6 activity on polymeric substrates was also assayed on an activity staining gel and by the analysis of the polynucleotide digestion products. The side by side comparison of the polynucleotide cleavage product profiles obtained by incubation with both RNase 6-H15A and RNase 7-H15A mutants, devoid of the main active site His, confirmed the presence in RNase 6 of another cleavage site. We observed that using the same assay conditions a considerable amount of activity is achieved with the RNase 6-H15A mutant, while non significant activity is observed for the corresponding RNase 7-H15A (Figure S4). Comparison of both RNases activity on

poly(C) together with RNase 6 mutants was also analyzed by the zymogram technique (Figure S2), where the RNase 6 double mutant display no detectable activity at even a 5 fold protein concentration. Interestingly, when comparing the poly(C) digestion pattern along with the His15 and 36 respective mutants' profiles we observe how both mutants shifted their product elution profile towards a more exonuclease type pattern, accumulating shorter intermediates than the native enzyme at an earlier stage of the reaction. A similar profile progression was previously reported for RNase 3, described to present a subsites arrangement that would favor an exonuclease cleavage pattern [20].

DISCUSSION

We report here the first crystal structure RNase 6 in complex with sulphate anions (Table 1). The location of putative phosphate binding sites was deduced from the position of the sulphate anions in the crystal structure (Figure 2 and Table S3). Structural analysis and kinetic characterization were carried out to outline the protein nucleotide binding sites arrangement. The first sulphate was ascribed to the main RNase phosphate binding site, shared with the other RNase A family members [54][55][67]. Two additional sulphate anions were located at the protein exposed cationic residues (His36/His39 and Arg66/His67) and would correspond to secondary phosphate binding sites. In particular, the His36/His39 site is proposed here as a novel and unique site within the RNase A family (Figures 1 and 3). Kinetic studies corroborated the involvement of His36 in the enzyme catalysis (Table 4).

The contribution of RNase 6 novel secondary catalytic site in the catalytic mechanism was further analysed by the characterization of the enzyme polynucleotide cleavage pattern (Figure 6). The distribution of substrate digestion products indicated that the breakdown of the polymeric substrate was not a random process. The chromatography profiles revealed the preference of RNase 6 for the binding and cleavage of long RNA strands, where the broken phosphodiester bonds would be located considerably spaced apart from the end of the chain. By comparison with the previously characterized RNase A cleavage pattern [29] we concluded that the RNase 6 activity toward the polymeric substrate was even more endonucleolytic than the previously described for RNase A [19]. On the other hand, we observed how the poly(C) digestion profile underwent a pronounced shift in its cleavage pattern towards an exonuclease type propensity when the main active site His was mutated (Figure 7).

Complementarily, structural analysis also illustrated a well defined substrate multisubsite arrangement for RNase 6. Interestingly, the predicted RNase 6 complex with an heptanucleotide by molecular dynamics (Figure 5) revealed the presence of novel sites at the RNA 5' end, that would be ascribed to B_{-2} and p_{-2}/p_{-3} sites (Table S5). Interestingly, the RNase 6 structure revealed equivalent His ND1 to NE2 atomic distances for His15/His122 and His36/His39, suggesting the presence of a secondary catalytic site. Besides, we observed stacking interactions between B_{-2} base of the the oligonucleotide and His39 in the predicted complex. However, structural analysis identified no additional residues for binding of adjacent bases at both phosphate sides. Notwithstanding, kinetic data on dinucleotides indicated a reduced efficiency performance for this novel active site. Indeed, the percentage of remnant catalytic activity displayed by the RNase 6-H15A mutant is similar to the activity displayed by a previously engineered RNase A construct with an additional active site created at the p_2 phosphate binding site position (RNase A-H7H10 variant) [49]. Likewise, a similar scenario might be envisaged for RNase 6 (see Table S6 for comparison of estimated pK_a values for both RNase A-His7/His10 and RNase 6-His36/His39 pairs). The calculated pK_a values for the corresponding His residues exposed at the protein surface indicated that neither of them underwent a significant decrease from the reference value that could provide an efficient base catalyst. Therefore, the predicted

pK_a for His36 and His 39 could not reproduce properly the efficient RNase A catalytic site [48][18]. And last but not least, the presence of a third residue that could stabilize the transition state intermediate is not obvious. Interestingly, we find a neighbouring Lys residue (Lys87) at the novel site environment that could meet the required RNase active site geometry (see Figure 3 for a schematic illustration). Unfortunately, Lys87 side chain is disordered in the present RNase 6 crystal structure, providing no information on its proper orientation. However, the Lys87 side conformation predicted by molecular dynamics in the RNase 6 –heptanucleotide complex did provide interactions to a phosphate located at the p_{-3} site (Table S5). Noteworthy, Lys87 is found in all primate RNase 6 counterparts but is absent in the murine sequence [9][15]. Interestingly, even if RNase A mutant at Lys41 was shown to drastically reduce the enzyme catalytic efficiency [70], the insertion of a secondary catalytic site for RNase A at p_2 location conformed by only a His dyad was also able to provide about a 10-15% of remnant activity in the absence of the main active site [49]. Likewise, the proposed novel RNase 6 secondary site would behave as a poor catalyst. In any case, the present kinetic data indicated that the presence of an anchoring site at the 36-39 region is enhancing significantly the enzyme catalysis of polymeric substrates. Interestingly, Sorrentino and co-workers analysis of the enzymatic properties of RNase A family members suggested that the presence of a cationic cluster at that region, combined with an anionic residue at RNase A residue at 83 position (Asp 80 in RNase 6), correlated to the facility to destabilize dsRNA, exposing single stranded stretches to the enzyme for cleavage[71][65][72]. Interestingly, RNase 6 shows a particular overabundance of His residues at its polypeptide sequence, in comparison to the other family homologues. As previously mentioned, most of these His residues are unique to RNase 6 lineage (Figure 1B) [9][15]. In particular, we observe two cationic clusters (His36/His39) and (Arg66/His67) fully conserved among the more evolved primate members. To note, while His36 and His67 are found in all known primate primary structures, His39 and Arg66 are only present in the more evolved primates. Overall, evolutionary pressure would have drifted RNase 6 towards a slightly more cationic primary structure with an overabundance of His residues, providing a novel secondary active site. Future research should explore the ultimate implications in the protein physiological function.

Conclusions

RNase 6 first crystal structure has provided us the opportunity to explore its structure - function relationship. By combining structural analysis together with molecular modelling and kinetic characterization, we were able to spot key regions contributing to the enzyme substrate specificity and catalytic properties. Results highlighted RNase 6 multisubsite arrangement for substrate binding and the contribution of a secondary catalytic site that facilitates the cleavage of polynucleotide substrates. Further work is envisaged to fully characterize RNase 6 enzymatic properties towards the understanding of its specific mechanism of action.

ACKNOWLEDGEMENTS

The authors wish to thank all the staff at the beamline BL13 (XALOC) at the ALBA Synchrotron Light Facility (Cerdanyola del Vallès, Spain) for their support during data collection. Heartfelt thanks to Jordi Joanhuix and Fernando Gil for all the help provided. Experimental work was supported by the *Ministerio de Economía y Competitividad* (grant BFU2012-38695) and *Generalitat de Catalunya* (grant 2014-SGR-728) and co-financed by FEDER funds. JAB was a recipient of a FPI predoctoral fellowship (*Ministerio de Economía y Competitividad*) and JA is a recipient of a PIF predoctoral fellowship (Universitat Autònoma de Barcelona).

DECLARATION OF INTEREST

There are no conflicts of interest to declare.

AUTHOR CONTRIBUTION

Ester Boix and Mohammed Moussaoui conceived and designed the experimental work. Guillem Prats-Ejarque, Javier Arranz-Trullen, Jose A Blanco, Mohammed Moussaoui and David Pulido performed the experiments. Guillem Prats-Ejarque, Mohammed Moussaoui, David Pulido, Victòria Nogués and Ester Boix analysed the data. Guillem Prats-Ejarque, Javier Arranz-Trullén, and Ester Boix drafted the paper. Victòria Nogués, Mohammed Moussaoui, Guillem Prats-Ejarque and Ester Boix revised the final manuscript.

REFERENCES

1 Boix, E. and Nogués, M. V. (2007) Mammalian antimicrobial proteins and peptides: overview on the RNase A superfamily members involved in innate host defence. Mol. Biosyst. **3**, 317–335.

2 Rosenberg, H. F. (2008) RNase A ribonucleases and host defense: an evolving story. J. Leukoc. Biol. **83**, 1079–1087.

3 Gupta, S. K., Haigh, B. J., Griffin, F. J. and Wheeler, T. T. (2012) The mammalian secreted RNases: Mechanisms of action in host defence. Innate Immun. **19**, 86–97.

4 Zhang, J. and Rosenberg, H. F. (2002) Complementary advantageous substitutions in the evolution of an antiviral RNase of higher primates. Proc. Natl. Acad. Sci. U. S. A. **99**, 5486–5491.

5 Pizzo, E. and D'Alessio, G. (2007) The success of the RNase scaffold in the advance of biosciences and in evolution. Gene **406**, 8–12.

6 Hamann, K. J., Ten, R. M., Loegering, D. A., Jenkins, R. B., Heise, M. T., Schad, C. R., Pease, L. R., Gleich, G. J. and Barker, R. L. (1990) Structure and chromosome localization of the human eosinophil-derived neurotoxin and eosinophil cationic protein genes: evidence for intronless coding sequences in the ribonuclease gene superfamily. Genomics **7**, 535–546.

7 Zhang, J., Dyer, K. D. and Rosenberg, H. F. (2002) RNase 8, a novel RNase A superfamily ribonuclease expressed uniquely in placenta. Nucleic Acids Res. **30**, 1169–1175.

8 Rosenberg, H. F. and Dyer, K. D. (1996) Molecular cloning and characterization of a novel human ribonuclease (RNase k6): increasing diversity in the enlarging ribonuclease gene family. Nucleic Acids Res. **24**, 3507–3513.

9 Deming, M. S., Dyer, K. D., Bankier, A. T., Piper, M. B., Dear, P. H. and Rosenberg, H. F. (1998) Ribonuclease k6: Chromosomal mapping and divergent rates of evolution within the RNase A gene superfamily. Genome Res. **8**, 599–607.

10 Becknell, B., Eichler, T. E., Beceiro, S., Li, B., Easterling, R. S., Carpenter, A. R., James, C. L., McHugh, K. M., Hains, D. S., Partida-Sanchez, S., et al. (2015) Ribonucleases 6 and 7 have antimicrobial function in the human and murine urinary tract. Kidney Int. **87**, 151–161.

11 Spencer, J. D., Schwaderer, a L., Wang, H., Bartz, J., Kline, J., Eichler, T., DeSouza, K. R., Sims-Lucas, S., Baker, P. and Hains, D. S. (2013) Ribonuclease 7, an antimicrobial peptide upregulated during infection, contributes to microbial defense of the human urinary tract. Kidney Int **83**, 615–625.

12 Jelicic, K., Cimbro, R., Nawaz, F., Huang, D. W., Zheng, X., Yang, J., Lempicki, R. A., Pascuccio, M., Van Ryk, D., Schwing, C., et al. (2013) The HIV-1 envelope protein gp120 impairs B cell proliferation by inducing TGF-beta1 production and FcRL4 expression. Nat. Immunol. **14**, 1256–1265.

13 Zhang, J., Dyer, K. D. and Rosenberg, H. F. (2000) Evolution of the rodent eosinophil-associated RNase gene family by rapid gene sorting and positive selection. Proc. Natl. Acad. Sci. U. S. A. **97**, 4701–4706.

14 McDevitt, A. L., Deming, M. S., Rosenberg, H. F. and Dyer, K. D. (2001) Gene structure and enzymatic activity of mouse eosinophil-associated ribonuclease 2. Gene **267**, 23–30.

15 Dyer, K. D., Rosenberg, H. F. and Zhang, J. (2004) Isolation, characterization, and evolutionary divergence of mouse RNase 6: evidence for unusual evolution in rodents. J. Mol. Evol. **59**, 657–665.

16 Richards, F. M. and Wyckoff, H. W. (1971) Bovine pancreatic ribonuclease. In Enzymes IV, pp647–806.

17 Raines, R. T. (1998) Ribonuclease A. Chem. Rev. **98**, 1045–1065.

18 Cuchillo, C. M., Nogués, M. V. and Raines, R. T. (2011) Bovine pancreatic ribonuclease: Fifty years of the first enzymatic reaction mechanism. Biochemistry **50**, 7835–7841.

19 Nogués, M. V., Moussaoui, M., Boix, E., Vilanova, M., Ribó, M. and Cuchillo, C. M. (1998) The contribution of noncatalytic phosphate-binding subsites to the mechanism of bovine pancreatic ribonuclease A. Cell. Mol. Life Sci. **54**, 766–774.

20 Boix, E., Nikolovski, Z., Moiseyev, G., Rosenberg, H. F., Cuchillo, C. M. and Nogues, M. V. (1999) Kinetic and product distribution analysis of human eosinophil cationic protein indicates a subsite arrangement that favors exonuclease-type activity. J. Biol. Chem. **274**, 15605–15614.

21 Rosenberg, H. F. (1995) Recombinant human eosinophil cationic protein. Ribonuclease activity is not essential for cytotoxicity. J. Biol. Chem. **270**, 7876–7881.

22 Harder, J. and Schroder, J.-M. (2002) RNase 7, a novel innate immune defense antimicrobial protein of healthy human skin. J. Biol. Chem. **277**, 46779–46784.

23 Boix, E., Salazar, V. a., Torrent, M., Pulido, D., Nogués, M. V. and Moussaoui, M. (2012) Structural determinants of the eosinophil cationic protein antimicrobial activity. Biol. Chem. **393**, 801–815.

24 Torrent, M., Sanchez, D., Buzon, V., Nogues, M. V, Cladera, J., Boix, E., Sánchez, D., Buzón, V., Nogués, M. V., Cladera, J., et al. (2009) Comparison of the membrane interaction mechanism of two antimicrobial RNases: RNase 3/ECP and RNase 7. Biochim. Biophys. Acta - Biomembr. **1788**, 1116–1125.

25 Libonati, M. and Sorrentino, S. (2001) Degradation of double-stranded RNA by mammalian pancreatic-type ribonucleases. Methods Enzymol. **341**, 234–248.

26 Bravo, J., Fernández, E., Ribó, M., Dellorens, R. and Cuchillo, C. M. (1994) A versatile negative-staining ribonuclease zymogram. Anal. Biochem. **219**, 82–86.

27 Moussaoui, M., Guasch, A., Boix, E., Cuchillo, C. M. and Nogués, M. V. (1996) The role of non-catalytic binding subsites in the endonuclease activity of bovine pancreatic ribonuclease A. J. Biol. Chem. **271**, 4687–4692.

28 Nogues, M. V and Cuchillo, C. M. (2001) Analysis by HPLC of distributive activities and the synthetic (back) reaction of pancreatic-type ribonucleases. Methods Mol. Biol. **160**, 15–24.

29 Cuchillo, C. M., Moussaoui, M., Barman, T., Travers, F. and Nogues, M. V. (2002) The exo- or endonucleolytic preference of bovine pancreatic ribonuclease A depends on its subsites structure and on the substrate size. Protein Sci. **11**, 117–128.

30 Kabsch, W. (2010) XDS. Acta Crystallogr. D. Biol. Crystallogr. **66**, 125–132.

31 Huang, Y. C., Lin, Y. M., Chang, T. W., Wu, S. H., Lee, Y. S., Chang, M. D., Chen, C., Wu, S. J. and Liao, Y. D. (2007) The flexible and clustered lysine residues of human ribonuclease 7 are critical for membrane permeability and antimicrobial activity. J. Biol. Chem. **282**, 4626–4633.

32 Adams, P. D., Afonine, P. V, Bunkoczi, G., Chen, V. B., Davis, I. W., Echols, N., Headd, J. J., Hung, L.-W., Kapral, G. J., Grosse-Kunstleve, R. W., et al. (2010) PHENIX: a comprehensive Python-based system for macromolecular structure solution. Acta Crystallogr. D. Biol. Crystallogr. **66**, 213–221.

33 Emsley, P. and Cowtan, K. (2004) Coot: model-building tools for molecular graphics. Acta Crystallogr. D. Biol. Crystallogr. **60**, 2126–2132.

34 Vaguine, A. A., Richelle, J. and Wodak, S. J. (1999) SFCHECK: a unified set of procedures for evaluating the quality of macromolecular structure-factor data

and their agreement with the atomic model. Acta Crystallogr. D. Biol. Crystallogr. **55**, 191–205.

35 Hooft, R. W., Vriend, G., Sander, C. and Abola, E. E. (1996) Errors in protein structures. Nature 23,381.

36 Pronk, S., Páll, S., Schulz, R., Larsson, P., Bjelkmar, P., Apostolov, R., Shirts, M. R., Smith, J. C., Kasson, P. M., Van Der Spoel, D., et al. (2013) GROMACS 4.5: A high-throughput and highly parallel open source molecular simulation toolkit. Bioinformatics **29**, 845–854.

37 Zegers, I., Maes, D., Poortmans, F., Palmer, R. and Wyns, L. (1994) The structures of RNase A complexed with 3 ' -CMP and d (CpA): Active site conformation and conserved water molecules. Protein Sci. 2322–2339.

38 Lindorff-Larsen, K., Piana, S., Palmo, K., Maragakis, P., Klepeis, J. L., Dror, R. O. and Shaw, D. E. (2010) Improved side-chain torsion potentials for the Amber ff99SB protein force field. Proteins **78**, 1950–1958.

39 Jorgensen, W. L., Chandrasekhar, J., Madura, J. D., Impey, R. W. and Klein, M. L. (1983) Comparison of simple potential functions for simulating liquid water. J. Chem. Phys. **79**, 926.

40 Darden, T., York, D. and Pedersen, L. (1993) Particle mesh Ewald: An N□log(N) method for Ewald sums in large systems. J. Chem. Phys. **98**, 10089.

41 Essmann, U., Perera, L., Berkowitz, M. L., Darden, T., Lee, H. and Pedersen, L. G. (1995) A smooth particle mesh Ewald method. J. Chem. Phys. **103**, 8577.

42 Hess, B. (2008) P-LINCS: A parallel linear constraint solver for molecular simulation. J. Chem. Theory Comput. **4**, 116–122.

43 Parrinello, M. and Rahman, A. (1981) Polymorphic transitions in single crystals: A new molecular dynamics method. J. Appl. Phys. **52**, 7182–7190.

44 Nosé, S. and Klein, M. L. (1983) Constant pressure molecular dynamics for molecular systems. Mol. Phys. **50**, 1055–1076.

45 Fontecilla-Camps, J. C., de Llorens, R., le Du, M. H. and Cuchillo, C. M. (1994) Crystal structure of ribonuclease A.d(ApTpApApG) complex. Direct evidence for extended substrate recognition. J. Biol. Chem. **269**, 21526–21531.

46 Morris, G. M., Huey, R., Lindstrom, W., Sanner, M. F., Belew, R. K., Goodsell, D. S. and Olson, A. J. (2009) AutoDock4 and AutoDockTools4: Automated docking with selective receptor flexibility. J. Comput. Chem. **30**, 2785–2791.

47 Kilambi, K. P. and Gray, J. J. (2012) Rapid calculation of protein pKa values using Rosetta. Biophys. J. **103**, 587–595.

48 Fisher, B. M., Schultz, L. W. and Raines, R. T. (1998) Coulombic effects of remote subsites on the active site of ribonuclease A. Biochemistry **37**, 17386–17401.

49 Moussaoui, M., Cuchillo, C. M. and Nogués, M. V. (2007) A phosphate-binding subsite in bovine pancreatic ribonuclease A can be converted into a very efficient catalytic site. Protein Sci. **16**, 99–109.

50 Krissinel, E. and Henrick, K. (2007) Inference of macromolecular assemblies from crystalline state. J. Mol. Biol. **372**, 774–797.

51 Rico, M., Gallego, E., Santoro, J., Bermejo, F. J., Nieto, J. L. and Herranz, J. (1984) On the fundamental role of the Glu 2- ... Arg 10+ salt bridge in the folding of isolated ribonuclease A S-peptide. Biochem. Biophys. Res. Commun., **123**, 757–763.

52 Chatani, E. and Hayashi, R. (2001) Functional and structural roles of constituent amino acid residues of bovine pancreatic ribonuclease A. J. Biosci. Bioeng., **92**, 98–107.

53 Berisio, R., Sica, F., Lamzin, V. S., Wilson, K. S., Zagari, a. and Mazzarella, L. (2002) Atomic resolution structures of ribonuclease A at six pH values. Acta Crystallogr. Sect. D Biol. Crystallogr., International Union of Crystallography **58**, 441–450.

54 Fedorov, A. A., Joseph-McCarthy, D., Fedorov, E., Sirakova, D., Graf, I. and Almo, S. C. (1996) Ionic interactions in crystalline bovine pancreatic ribonuclease A. Biochemistry **35**, 15962–15979.

55 Leonidas, D. D., Boix, E., Prill, R., Suzuki, M., Turton, R., Minson, K., Swaminathan, G. J., Youle, R. J. and Acharya, K. R. (2001) Mapping the ribonucleolytic active site of eosinophil-derived neurotoxin (EDN): High resolution crystal structures of EDN complexes with adenylic nucleotide inhibitors. J. Biol. Chem. **276**, 15009–15017.

56 Boix, E., Pulido, D., Moussaoui, M., Nogues, M. V. and Russi, S. (2012) The sulfate-binding site structure of the human eosinophil cationic protein as revealed by a new crystal form. J. Struct. Biol. **179**, 1–9.

57 Holloway, D. E., Chavali, G. B., Hares, M. C., Subramanian, V. and Acharya, K. R. (2005) Structure of murine angiogenin: features of the substrate- and cell-binding regions and prospects for inhibitor-binding studies. Acta Crystallogr. D. Biol. Crystallogr. **61**, 1568–1578.

58 Borkakoti, N. (1983) The active site of ribonuclease A from the crystallographic studies of ribonuclease-A-inhibitor complexes. Eur. J. Biochem. **132**, 89–94.

59 Berisio, R., Lamzin, V. S., Sica, F., Wilson, K. S., Zagari, A. and Mazzarella, L. (1999) Protein titration in the crystal state. J. Mol. Biol. **292**, 845–854.

60 deMel, V. S., Martin, P. D., Doscher, M. S. and Edwards, B. F. (1992) Structural changes that accompany the reduced catalytic efficiency of two semisynthetic ribonuclease analogs. J. Biol. Chem. **267**, 247–256.

61 Schultz, L. W., Quirk, D. J. and Raines, R. T. (1998) His...Asp catalytic dyad of ribonuclease A: structure and function of the wild-type, D121N, and D121A enzymes. Biochemistry **37**, 8886–8898.

62 Hofsteenge, J., Vicentini, a. and Zelenko, O. (1998) Ribonuclease 4, an evolutionarily highly conserved member of the superfamily. Cell. Mol. Life Sci. **54**, 804–810.

63 Vicentini, A. M., Kote-Jarai, Z. and Hofsteenge, J. (1996) Structural determinants of the uridine-preferring specificity of RNase PL3. Biochemistry **35**, 9128–9132.

64 Terzyan, S. S., Peracaula, R., de Llorens, R., Tsushima, Y., Yamada, H., Seno, M., Gomis-Ruth, F. X. and Coll, M. (1999) The three-dimensional structure of human RNase 4, unliganded and complexed with d(Up), reveals the basis for its uridine selectivity. J. Mol. Biol. **285**, 205–214.

65 Sorrentino, S. (1998) Human extracellular ribonucleases: Multiplicity, molecular diversity and catalytic properties of the major RNase types. Cell. Mol. Life Sci. **54**, 785–794.

66 Sorrentino, S. (2010) The eight human “canonical” ribonucleases: Molecular diversity, catalytic properties, and special biological actions of the enzyme proteins. FEBS Lett. **584**, 2194–2200.

67 Boix, E., Blanco, J. a., Nogués, M. V. and Moussaoui, M. (2013) Nucleotide binding architecture for secreted cytotoxic endoribonucleases. Biochimie **95**, 1087–1097.

68 Vitagliano, L., Merlino, A., Zagari, A. and Mazzarella, L. (2000) Productive and nonproductive binding to ribonuclease A: X-ray structure of two complexes with uridylyl(2’,5')guanosine. Protein Sci. **9**, 1217–1225.

69 Park, C., Schultz, L. W. and Raines, R. T. (2001) Contribution of the active site histidine residues of ribonuclease A to nucleic acid binding. Biochemistry **40**, 4949–4956.

70 Trautwein, K., Holliger, P., Stackhouse, J. and Benner, S. A. (1991) Site-directed mutagenesis of bovine pancreatic ribonuclease: lysine-41 and aspartate-121. FEBS Lett. **281**,275–277.

71 Libonati, M. and Sorrentino, S. (1992) Revisiting the action of bovine ribonuclease A and pancreatic-type ribonucleases on double-stranded RNA. Mol. Cell. Biochem. **117**, 139–151.

72 Yakovlev, G., Moiseyev, G. P., Sorrentino, S., De Prisco, R. and Libonati, M. (1997) Single-strand-preferring RNases degrade double-stranded RNAs by destabilizing its secondary structure. J. Biomol. Struct. Dyn. **15**, 243–250.

73 Shapiro, R., Fett, J. W., Strydom, D. J. and Vallee, B. L. (1986) Isolation and characterization of a human colon carcinoma-secreted enzyme with pancreatic ribonuclease-like activity. Biochemistry **25**, 7255–7264.

74 Follmann, H., Wieker, H. J. and Witzel, H. (1967) [On the mechanism of the ribonuclease reaction. 2. The pre-ordering in the substrate as the accelerating factor in cinucleoside phosphates and analagous compounds]. Eur. J. Biochem., **1**, 243–250.

75 Boix, E., Nogues, M. V., Schein, C. H., Benner, S. a and Cuchillo, C. M. (1994) Reverse Transphosphorylation by Ribonuclease A Needs an Intact p2 -binding Site. J. Biol. Chem. **269**, 2529–2534.

76 Sorrentino, S. and Glitz, D. G. (1991) Ribonuclease activity and substrate preference of human eosinophil cationic protein (ECP). FEBS Lett. **288**, 23–26.

77 Pettersen, E. F., Goddard, T. D., Huang, C. C., Couch, G. S., Greenblatt, D. M., Meng, E. C. and Ferrin, T. E. (2004) UCSF Chimera - A visualization system for exploratory research and analysis. J. Comput. Chem. **25**, 1605–1612.

TABLES

Table 1: Data collection, processing and structure refinement parameters for the RNase 6 crystal structure (PDB ID: 4X09).

Data collection		***Refinement***	
Space group	$P2_12_12_1$	Resolution range (Å)	48.98 – 1.72
Unit cell		R_{cryst} [c] / R_{free} [d] (%)	19.28 / 22.67
a, b, c (Å)	27.73 38.86 97.97	No. of protein atoms	1068
α, β, γ (°)	90.0 90.0 90.0	No. of water molecules	124
No. of molecules in a.u.	1	No. of bound anions	4
Resolution (Å)	1.72	R.m.s. deviation from ideality	
No. of total reflections	22981	In bond lengths (Å)	0.004
No. of unique reflections	11717	In bond angles (deg)	0.908
R_{merge} [a, b] (%)	2.8 (23.4)	Average B factors (Å^2)	
I/σ_I [b]	13.0 (2.4)	All protein atoms	30.34
Completess for range [b] (%)	99.2 (99.0)	Main chain atoms	27.30
Wilson B factor (Å^2)	24.7	Side chain atoms	33.23
Matthews coefficient (Å^3/Da)	1.80	Sulphate anion atoms	57.60
Solvent content (%)	31.71	Glycerol atoms	49.55
		Water molecules	40.67

[a] R_{merge}= Σ_{hkl} Σ_{j-1} to N$|I_{hkl}-I_{hkl}(j)|$/ Σ_{hkl} Σ_{j-1} to N $I_{hkl}(j)$, where N is the redundancy of the data.

[b] Outermost shell is 1.78-1.72 Å.

[c] $R_{crystal}$= $\Sigma_h|F_o-F_c|/\Sigma_h F_o$, where F_o and F_c are the observed and calculated structure factor amplitudes of reflection h, respectively.

[d] R_{free} is equal to R_{cryst} for a randomly selected 5% subset of reflections not used in the refinement.

Table 2. Kinetic parameters of RNases for dinucleotide and mononucleotide cyclic phosphate substrates.

		UpA	UpG	CpA	C>p
RNase 6	K_m (mM) [a]	2.63± 0.3	ND	1.22 ± 0.2	2.06 ± 0.3
	k_{cat} (s^{-1})	12.9 ± 1.1	ND	1.08 ± 0.1	3.25×10^{-3} ± 0.06
	k_{cat}/K_m ($s^{-1} M^{-1}$)	4.90×10^3	ND	8.85×10^2	1.60
RNase 3	K_m (mM)	2.7 ± 0.66	ND	1.7 ± 0.3	3 ± 0.53
	k_{cat} (s^{-1})	1.22 ± 0.12	ND	0.55 ± 0.06	$3.2 \times 10^{-3} \pm 5.1 \times 10^{-4}$
	k_{cat}/K_m ($s^{-1} M^{-1}$)	4.47×10^2	ND	3.23×10^2	1.07
RNase A [b]	K_m (mM)	0.7	2.0	0.5	1.06 ± 0.1
	k_{cat} (s^{-1})	2.69×10^3	1.38×10^2	2.3×10^3	2.28 ± 0.18
	k_{cat}/K_m ($s^{-1} M^{-1}$)	3.84×10^6	6.9×10^4	4.59×10^6	2.15×10^3

[a] All assays were carried out in duplicates by a spectrophometric assay as described in the methodology. Kinetic parameters were estimated from nonlinear regression data using the *GraFit* program.

[b] Values shown for RNase A activity are taken from [73][74][75].

ND: Not detected at the assayed conditions.

Table 3. Catalytic activity ratio of RNases for the assayed nucleotides.

	CpA/UpA	CpA/C>p	Poly(C)/Poly(U)	Poly (U)/Poly(U):Poly(A)
RNase 6	0.18	$5.5x10^2$	1.02	0.43
RNase 3	0.72	$3.0\ x10^2$	1.74	ND
RNase A [a]	1.20	$2.1x10^3$	8.14	307

ND: Not detected at the assayed conditions.
[a] Data for Poly(U):Poly(A) were taken from [76].

Table 4.Relative catalytic activities for wild-type RNases 6 and 7 and mutant variants.

	UpA	CpA	Poly (U)	Poly(U):Poly(A)
RNase 6	100	100	100	100
RNase 6-H15A[a]	13	14	77	63
RNase 6-H36R	94	86	36	40
RNase 6-H15A/H36A	ND	ND	15	5
RNase 7	100	100	100	100
RNase 7-H15A	ND	ND	3	7

ND: Not detected at the assayed conditions.

[a]Data expressed in percentage of activity in relation to the wild-type protein (%). Mean values were calculated from triplicate assays, showing in all cases a standard error below 10%.

FIGURE LEGENDS

Figure 1: (A) Structure-based sequence of the eight canonical human RNases together with RNase A. The active sites are highlighted in yellow. The four disulphide bonds are labelled with green numbers. Tested mutations on RNase 6 are pointed with red arrows. The alignment was performed using *ClustalW,* and the picture was drawn using *ESPript (*http://espript.ibcp.fr/ESPript*/).* Labels are as follows: red box, white character –for strict identity; red character for similarity in a group and character with blue frame for similarity across groups. B) RNase 6 three-dimensional structure surface representation using the *CONSURF* web server (http://consurf.tau.ac.il/) featuring the relationships among the evolutionary conservation of amino acid positions within the RNase A family. The three-dimensional structure shows residues coloured by their conservation score using the colour-coding bar at the bottom image. Sulphate anions (S1-S4) and the glycerol (GOL) molecule found in the crystal structure are depicted. Conserved residues belonging to the RNase catalytic site and interacting with bound sulphate anions are labelled.

Figure 2: Detail of RNase 6 interactions with sulphate bound molecules. Atoms involved in the protein –anion interactions are listed in Table S3. The sulphate involved in the crystal packing (S3) is not shown here. The picture was drawn with *PyMol* 1.7.2 (DeLano Scientific).

Figure 3: Illustrative scheme of the RNase 6 main active site (A) and the putative secondary site (B). CA atom distances are labelled together with the His ND1 to NE2 respective distances. The figure was created with *Pymol* (Delano scientific).

Figure 4. Predicted structure of RNase 6 and RNase A in complex with CpA, UpA and UpG dinucleotides after molecular dynamics simulations, as detailed in the methodology. Nucleotides are coloured in green. RNases interacting residues are coloured in magenta. Hydrogen bonds are coloured in yellow. Pictures were drawn with *UCSF Chimera 1.10*[77].

Figure 5. RNase 6 in complex with CCCAUAA heptanucleotide after a molecular dynamics simulation, as described in the methodology. The heptanucleotide is coloured in green. The heptanucleotide is coloured in green. Interacting residues of RNase 6 are coloured in turquoise. Protein interacting residues and ligand atoms are coloured according to their element. Hydrogen bonds are coloured in yellow. Overlapped sulphate ions of the original coordinates of the crystal are coloured in magenta. The picture was drawn with *UCSF Chimera 1.10*.

Figure 6. Poly(C) cleavage pattern obtained by RNase 6 (A) compared to RNase A[27] (B). Chromatography profiles of poly(C) digestion products are shown at selected incubation times corresponding to representative steps of the catalysis process. See “Materials and methods” for substrate digestion conditions.

Figure 7. Poly(C) cleavage pattern by RNase 6-H15A (A) and RNase 6-H36R (B) mutants. Chromatography profiles of poly(C) digestion products are shown at selected incubation times corresponding to representative steps of the catalysis process.

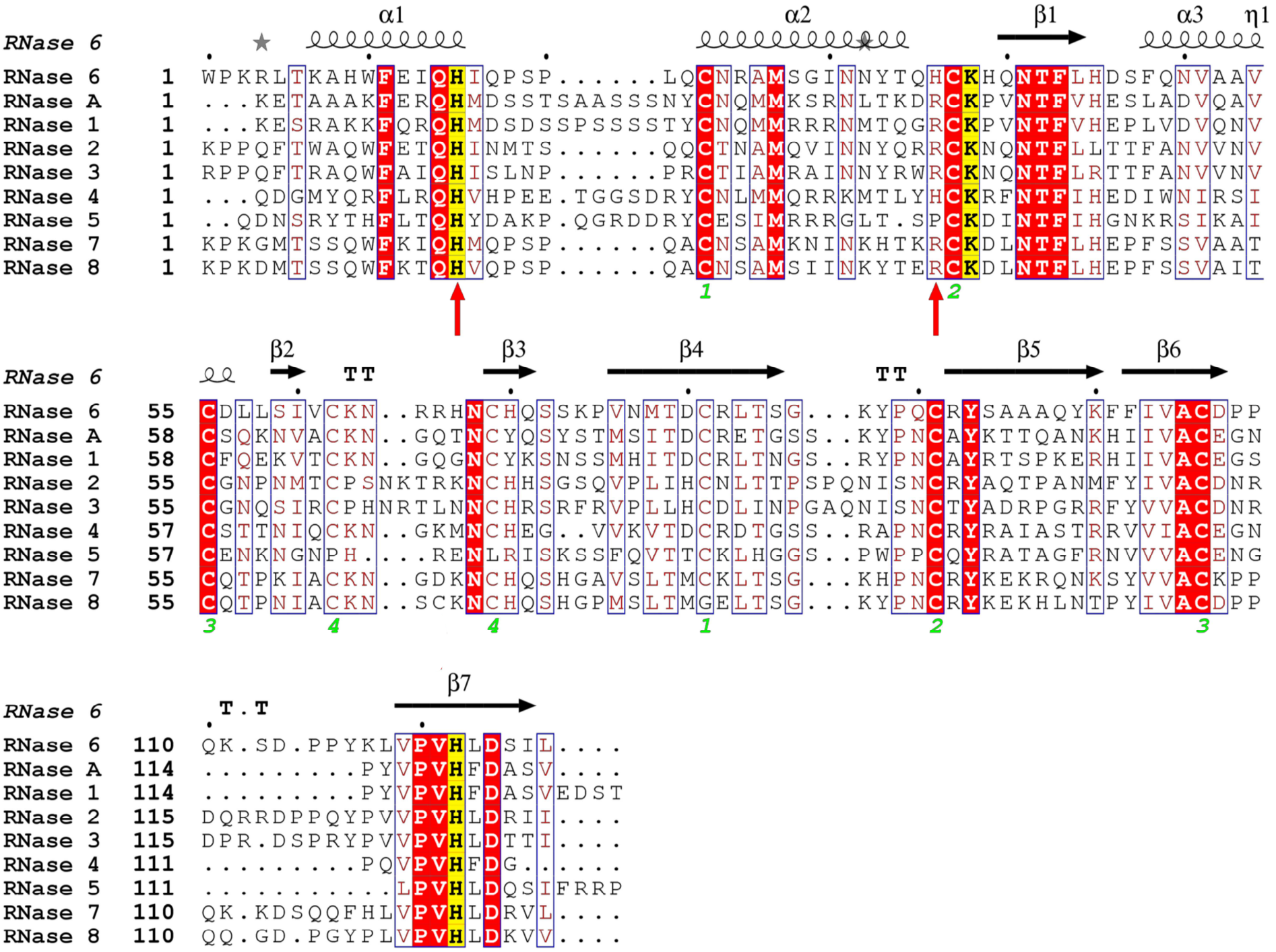
α1
α2
β1
α3
η1
RNase 6
RNase 6 1 WPKRLTKAHWFEIQHIQPSP.....LQCNRAMSGINNYTQHCKHQNTFLHDSFQNVAAV
RNase A 1 ...KETAAAKFERQHMDSSTSAASSSNYCNQMMKSRNLTKDRCKPVNTFVHESLADVQAV
RNase 1 1 ...KESRAKKFQRQHMDSDSSPSSSSTYCNQMMRRRNMTQGRCKPVNTFVHEPLVDVQNV
RNase 2 1 KPPQFTWAQWFETQHINMTS.....QQCTNAMQVINNYQRRCKNQNTFLLTTFANVVNV
RNase 3 1 RPPQFTRAQWFAIQHISLNP.....PRCTIAMRAINNYRWRCKNQNTFLRTTFANVVNV
RNase 4 1 ...QDGMYQRFLRQHVHPEE.TGGSDRYCNLMMQRRKMTLYHCKRFNTFIHEDIWNIRSI
RNase 5 1 ..QDNSRYTHFLTQHYDAKP.QGRDDRYCESIMRRRGLT.SPCKDINTFIHGNKRSIKAI
RNase 7 1 KPKGMTSSQWFKIQHMQPSP.....QACNSAMKNINKHTKRCKDLNTFLHEPFSSVAAT
RNase 8 1 KPKDMTSSQWFKTQHVQPSP.....QACNSAMSIINKYTERCKDLNTFLHEPFSSVAIT
1
2
β2
β3
β4
β5
β6
RNase 6
RNase 6 55 CDLLSIVCKN..RRHNCHQSSKPVNMTDCRLTSG...KYPQCRYSAAAQYKFFIVACDPP
RNase A 58 CSQKNVACKN..GQTNCYQSYSTMSITDCRETGSS..KYPNCAYKTTQANKHIIVACEGN
RNase 1 58 CFQEKVTCKN..GQGNCYKSNSSMHITDCRLTNGS..RYPNCAYRTSPKERHIIVACEGS
RNase 2 55 CGNPNMTCPSNKTRKNCHHSGSQVPLIHCNLTTPSPQNISNCRYAQTPANMFYIVACDNR
RNase 3 55 CGNQSIRCPHNRTLNNCHRSRFRVPLLHCDLINPGAQNISNCTYADRPGRRFYVVACDNR
RNase 4 57 CSTTNIQCKN..GKMNCHEG..VVKVTDCRDTGSS..RAPNCRYRAIASTRRVVIACEGN
RNase 5 57 CENKNGNPH...RENLRISKSSFQVTTCKLHGGS..PWPPCQYRATAGFRNVVVACENG
RNase 7 55 CQTPKIACKN..GDKNCHQSHGAVSLTMCKLTSG...KHPNCRYKEKRQNKSYVVACKPP
RNase 8 55 CQTPNIACKN..SCKNCHQSHGPMSLTMGELTSG...KYPNCRYKEKHLNTPYIVACDPP
3
4
4
1
2
3
β7
RNase 6
RNase 6 110 QK.SD.PPYKLVPVHLDSIL....
RNase A 114 ....PYVPVHFDASV....
RNase 1 114 .........PYVPVHFDASVEDST
RNase 2 115 DQRRDPPQYPVVPVHLDRII....
RNase 3 115 DPR.DSPRYPVVPVHLDTTI....
RNase 4 111 ....PQVPVHFDG.....
RNase 5 111 ..........LPVHLDQSIFRRP
RNase 7 110 QK.KDSQQFHLVPVHLDRVL....
RNase 8 110 QQ.GD.PGYPLVPVHLDKVV....

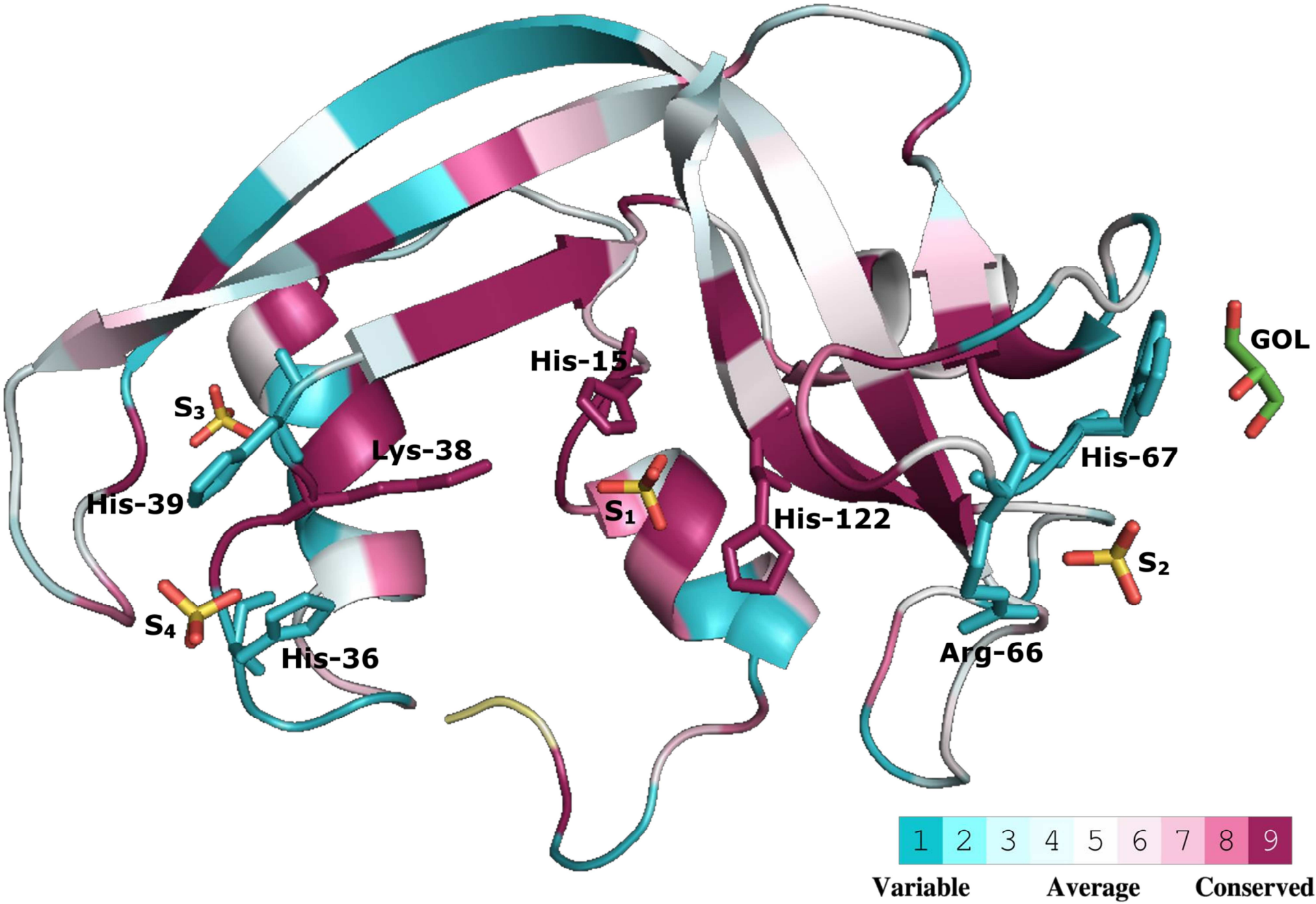
His-15
S3
Lys-38
His-39
S1
His-122
His-67
GOL
S2
S4
His-36
Arg-66
1 2 3 4 5 6 7 8 9
Variable
Average
Conserved

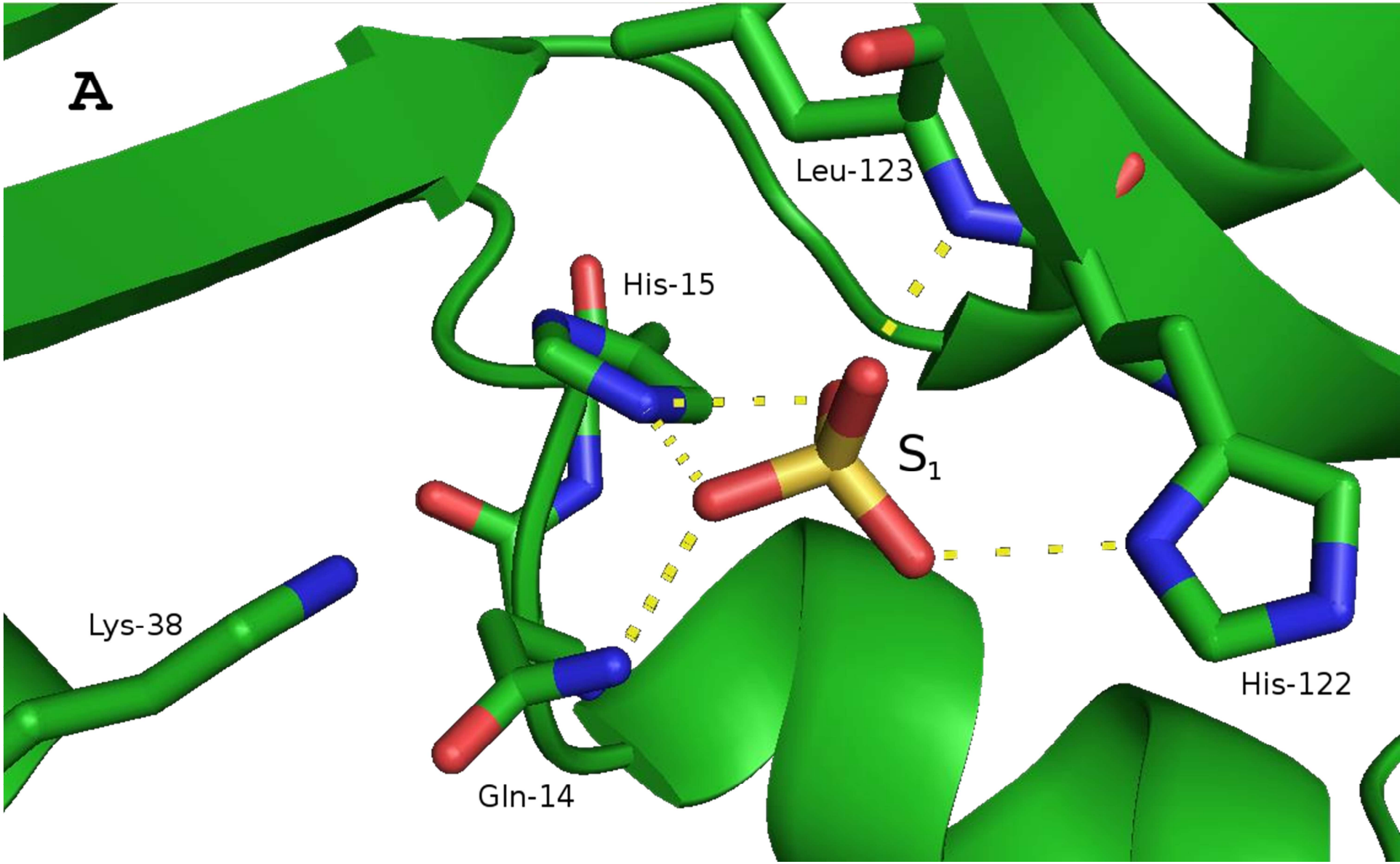
A
Leu-123
His-15
S1
Lys-38
His-122
Gln-14

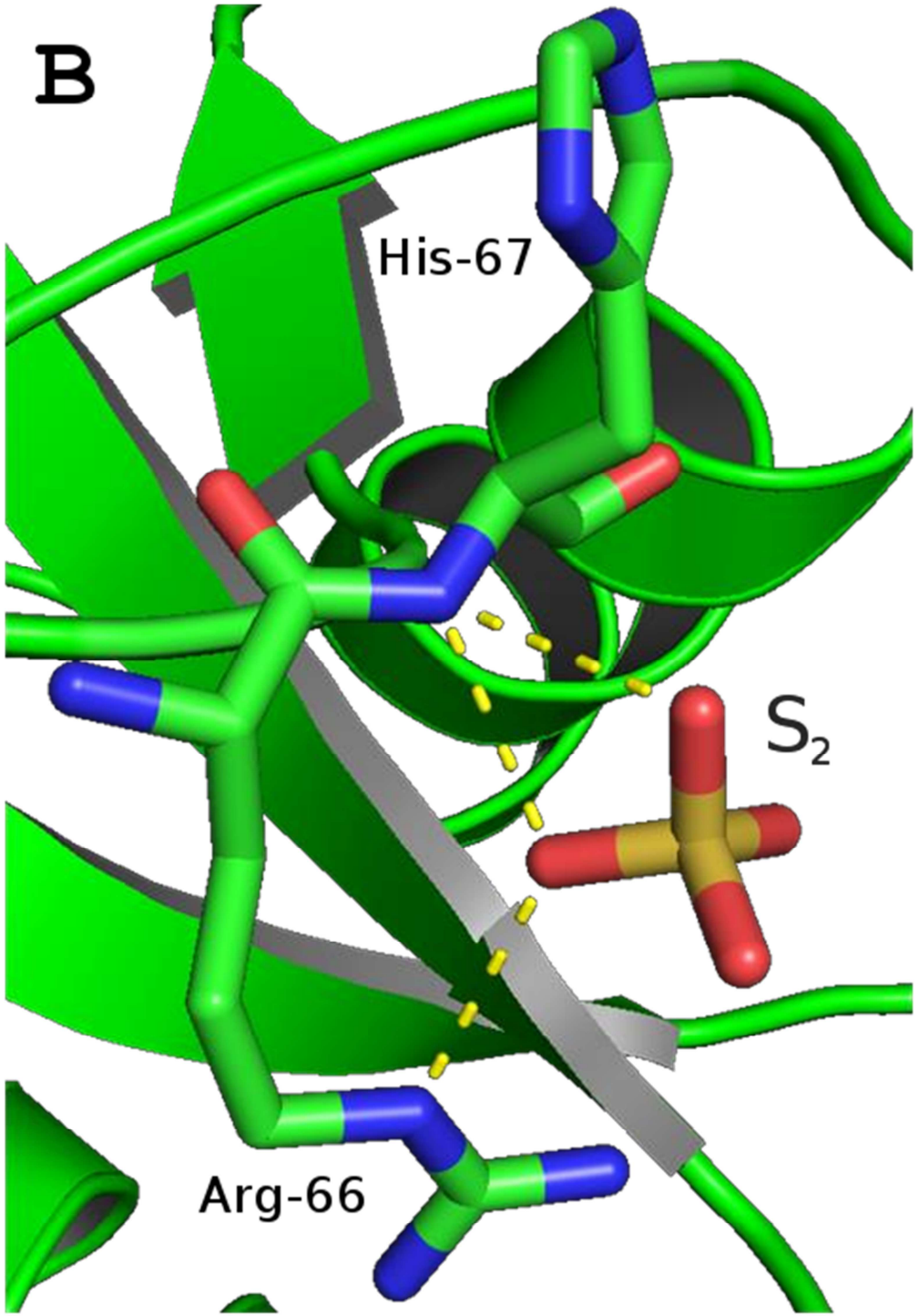
B
His-67
S_2
Arg-66

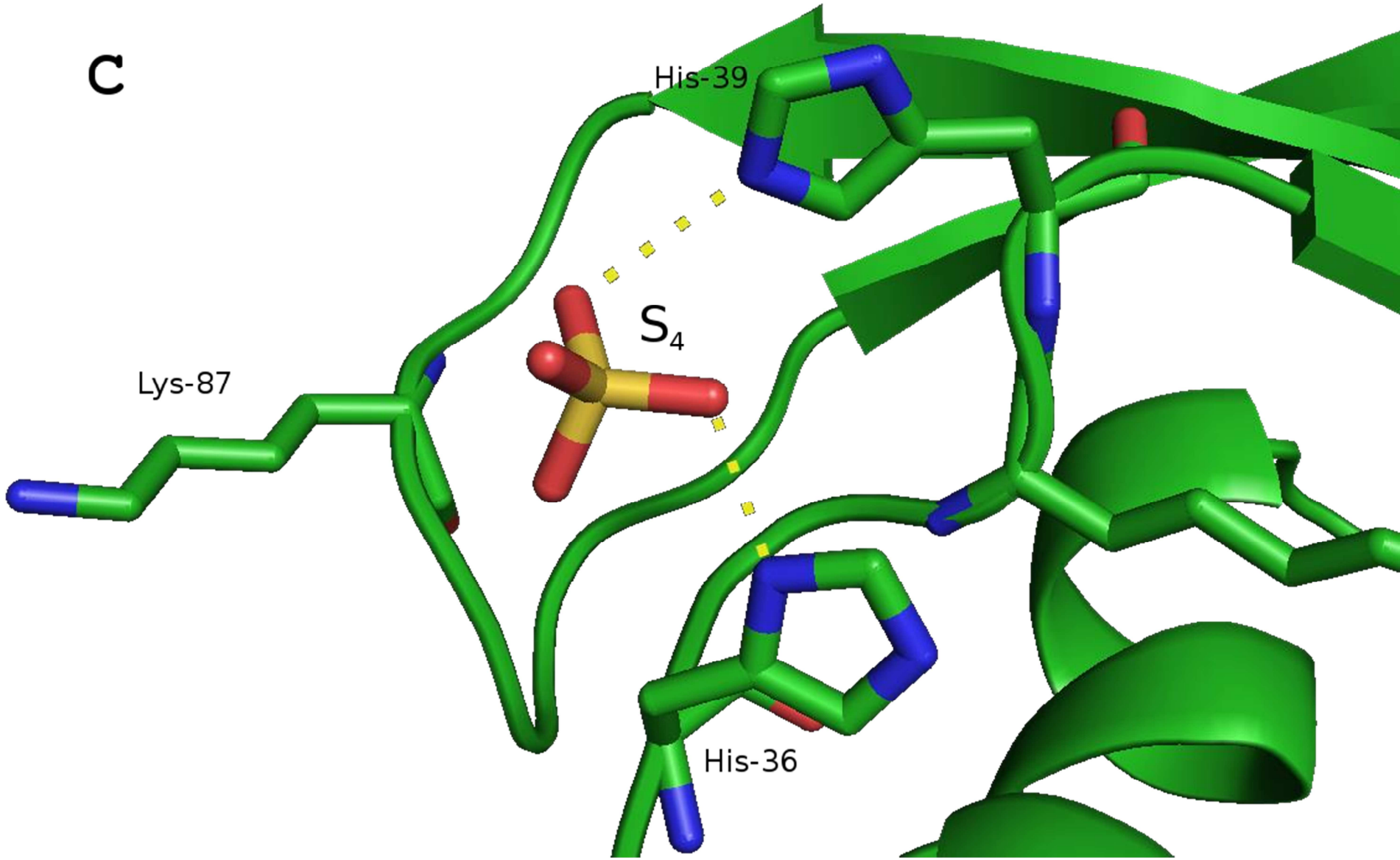
C
His-39
S_4
Lys-87
His-36

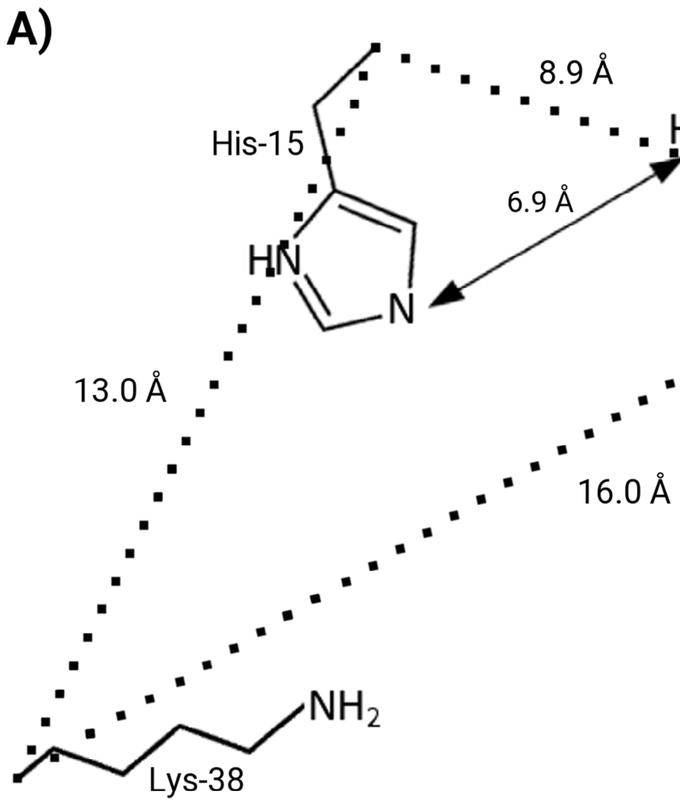
A)
His-15
8.9 Å
HN
N
His-122
6.9 Å
HN
N
13.0 Å
16.0 Å
NH2
Lys-38

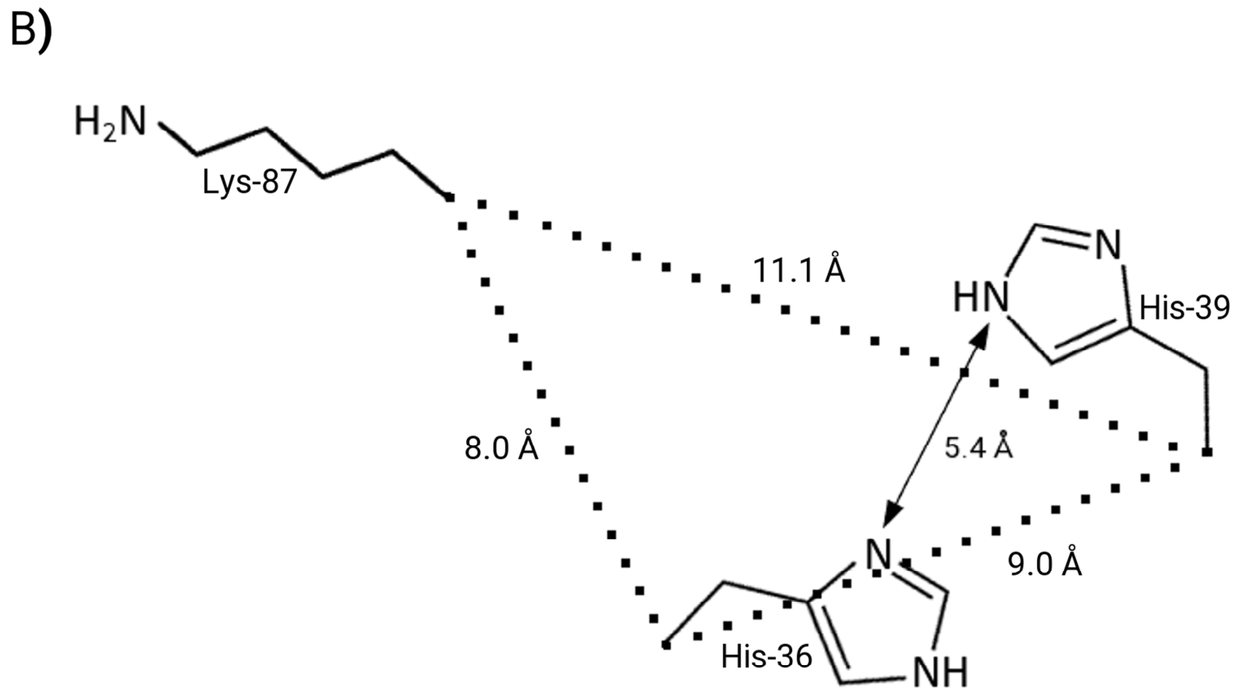
B)
H2N
Lys-87
11.1 Å
HN
N
His-39
8.0 Å
5.4 Å
9.0 Å
N
His-36
NH

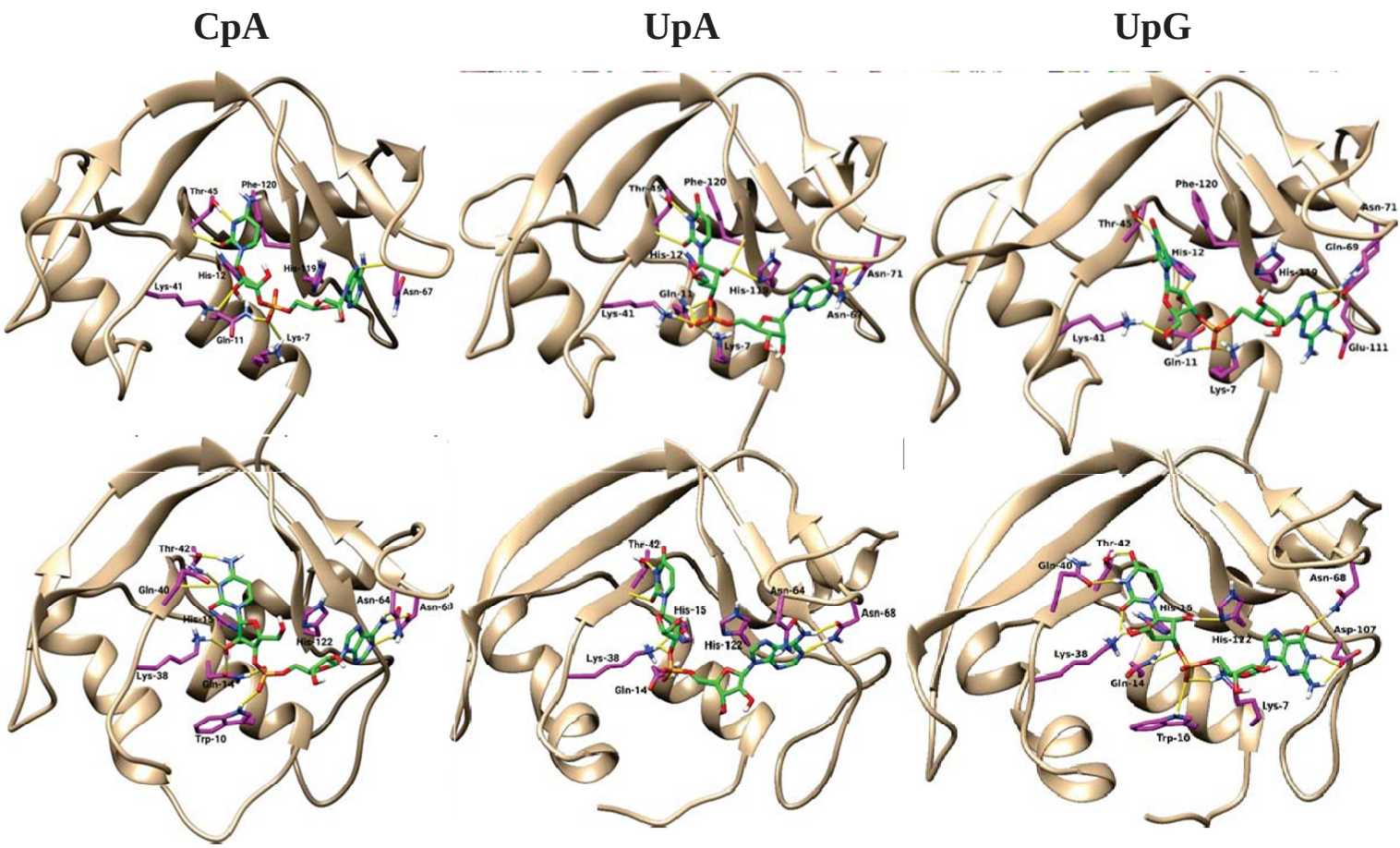
CpA
UpA
UpG
RNase A
RNase 6
Thr-45
Phe-120
His-12
His-119
Lys-41
Gln-11
Lys-7
Asn-67
Asn-71
Gln-69
Glu-111
Thr-42
Gln-40
His-15
His-122
Asn-64
Asn-63
Asn-68
Lys-38
Gln-14
Trp-10
Asp-107

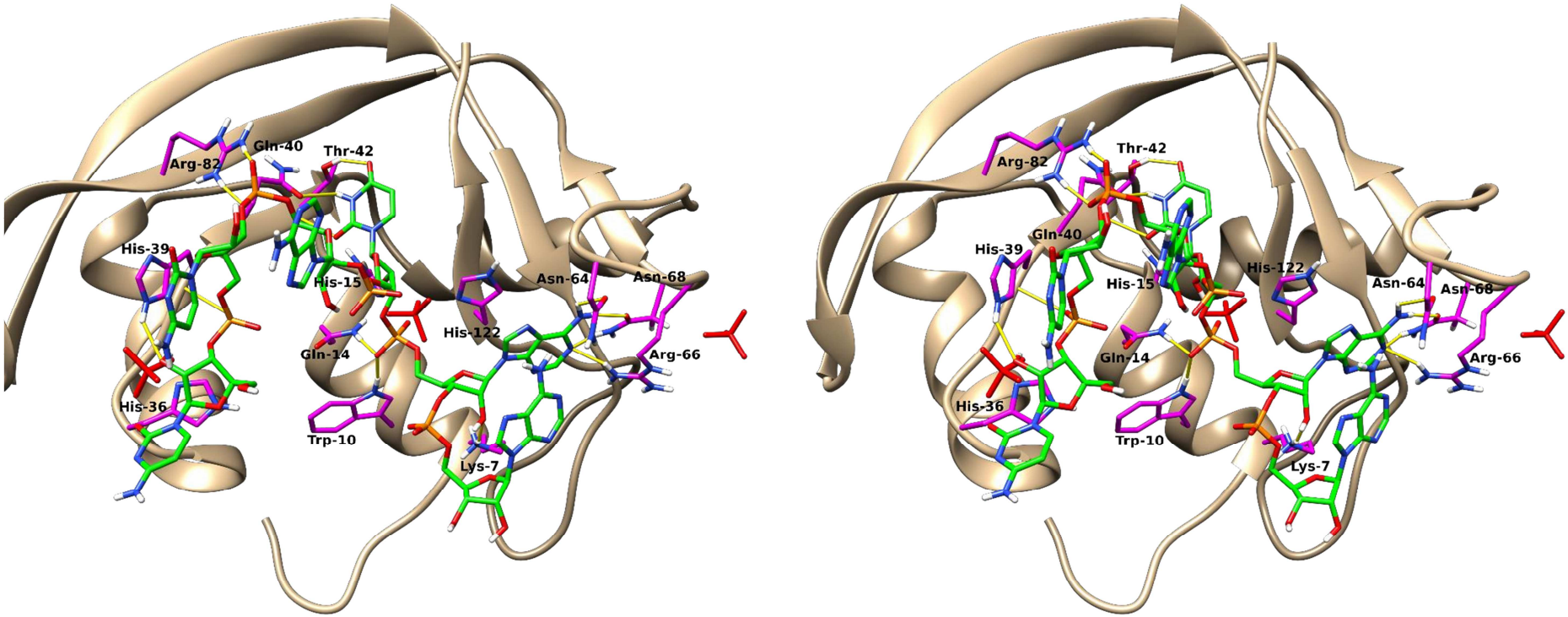
Arg-82
Gln-40
Thr-42
His-39
His-15
Asn-64
Asn-68
His-122
Gln-14
Arg-66
His-36
Trp-10
Lys-7
Arg-82
Thr-42
Gln-40
His-39
His-15
His-122
Asn-64
Asn-68
Gln-14
Arg-66
His-36
Trp-10
Lys-7

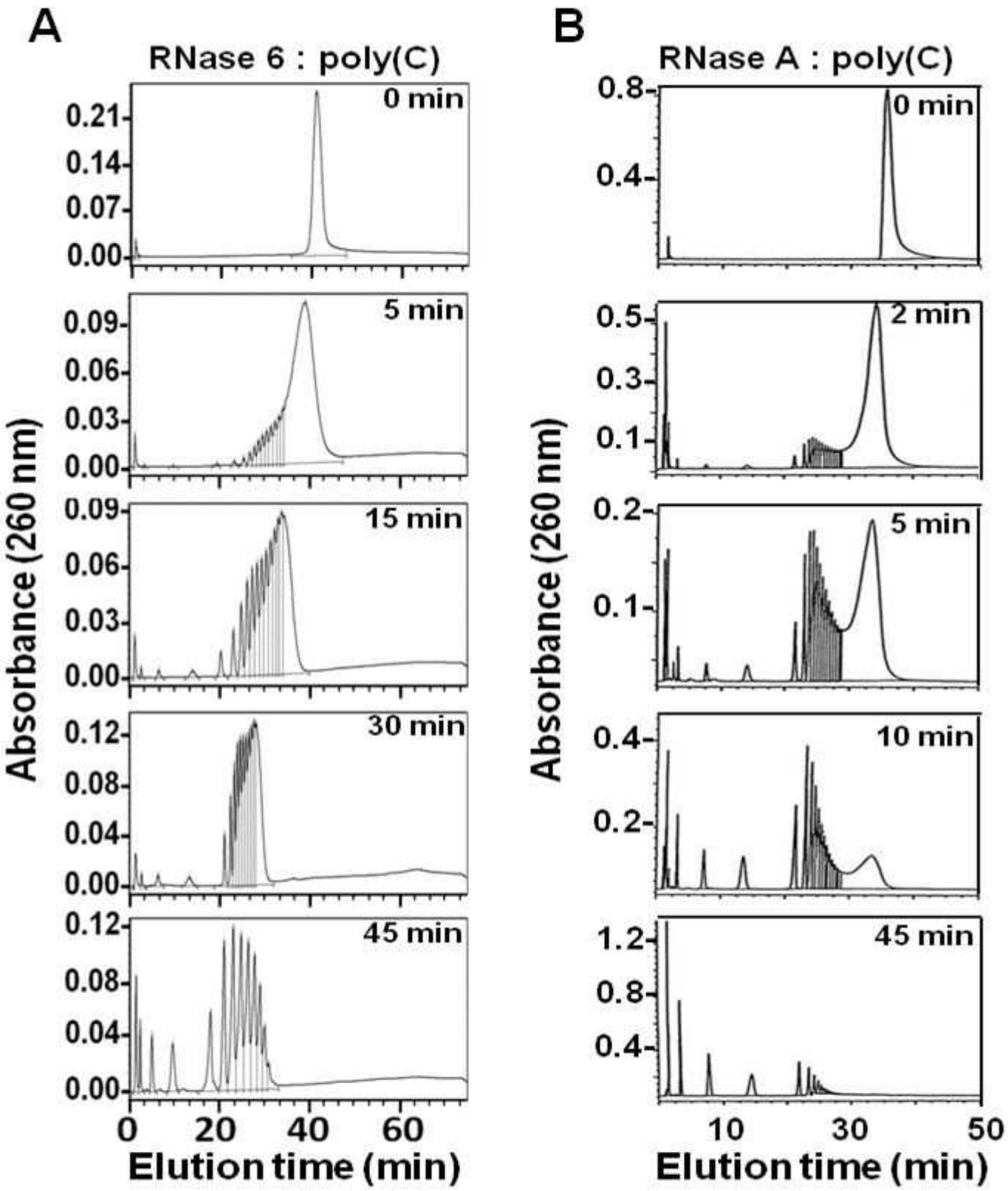
A
RNase 6 : poly(C)
0 min
5 min
15 min
30 min
45 min
Absorbance (260 nm)
Elution time (min)
B
RNase A : poly(C)
0 min
2 min
5 min
10 min
45 min
Absorbance (260 nm)
Elution time (min)

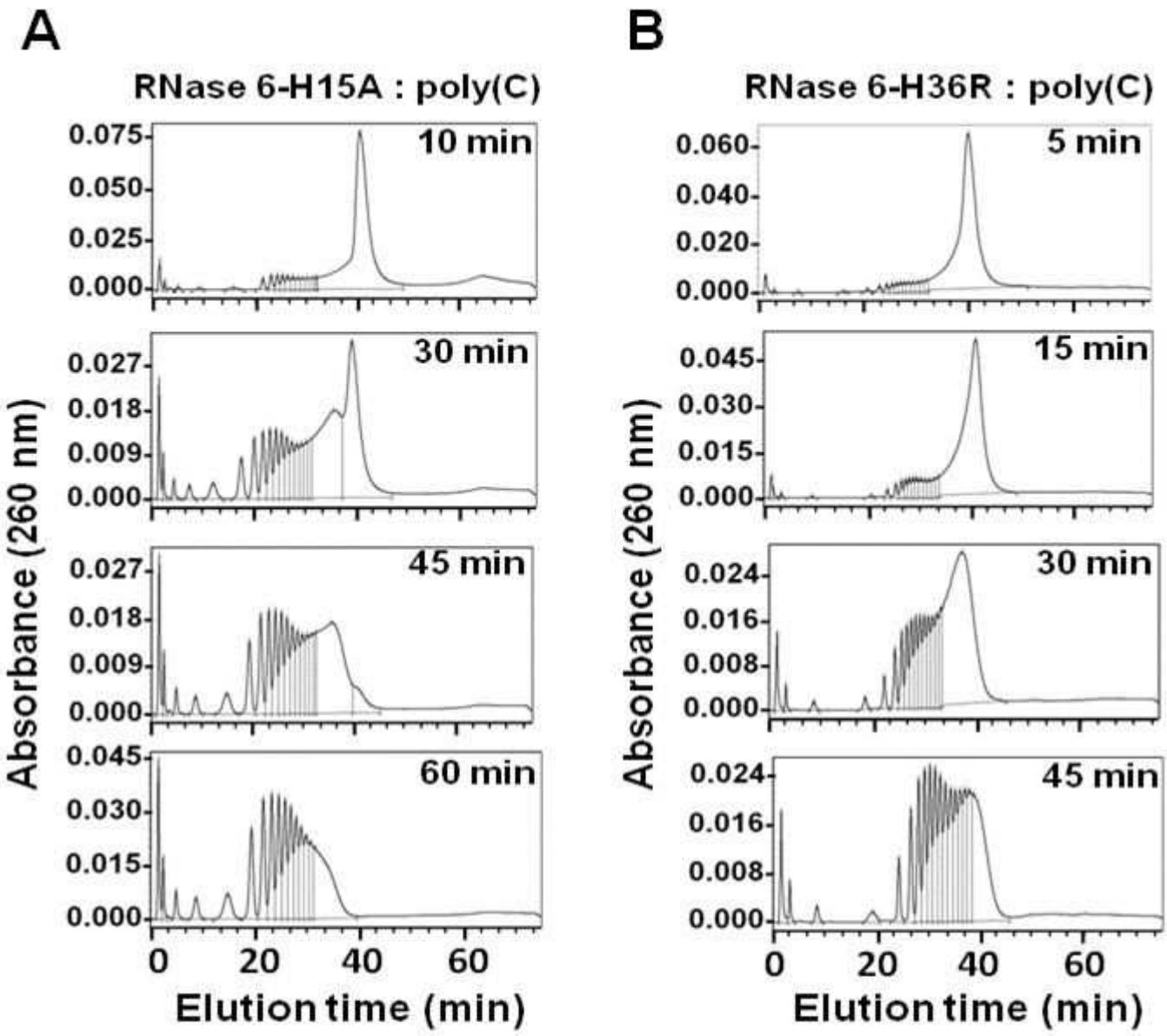
A
RNase 6-H15A : poly(C)
10 min
30 min
45 min
60 min
0.075
0.050
0.025
0.000
0.027
0.018
0.009
0.045
0.030
0.015
Absorbance (260 nm)
0
20
40
60
Elution time (min)
B
RNase 6-H36R : poly(C)
5 min
15 min
30 min
45 min
0.060
0.040
0.020
0.024
0.016
0.008
Absorbance (260 nm)
0
20
40
60
Elution time (min)

Title: The first crystal structure of human RNase 6 reveals a novel substrate binding and cleavage site arrangement. Authors: Prats-Ejarque[1] G, Arranz-Trullén[1] J; Blanco[1] JA; Pulido[1,2] D; Nogués[1] MV; Moussaoui[1] M; and Boix[1] E[¶].

[1] Department of Biochemistry and Molecular Biology, Faculty of Biosciences, Universitat Autònoma de Barcelona, E-08193 Cerdanyola del Vallès, Spain
[2] Present address: Imperial College London, South Kensington Campus London, London SW7 2AZ, United Kingdom

[¶]Author to whom correspondence should be addressed; E-Mail ester.boix@uab.cat; Tel.: +34-93-581-2565; Fax: +34-93-581-1264

Supplementary Material content:

Structure validation report for RNase 6 crystal structure (PDB ID: 4X09).

Table S1: RNase 6 secondary structure elements.

loop residues		***helix residues***		***strand residues***	
L1	W1 – T6	α1	K7 – H15	β1	Q40 – L44
L2	I16 – Q22	α2	C23 – T34	β2	S59 – I60
L3	Q35 – H39	α3	F48 – D56	β3	C69 – Q71
L4	H45 – S47			β4	V76 – S85
L5	L57 – L58			β5	R92 – K100
L6	V61 – N68			β6	F102 – D107
L7	S72 – P75			β7	V119 – I126
L8	G86 – C91				
L9	P108– L118				

Table S2: Intermolecular packing interactions between symmetry related molecules in the RNase 6 crystal. Only hydrogen bond interactions are included, taking a cut-off of 3.4 Å as a reference, as calculated by the *PDBePISA* server [1].

symmetry operation	***crystal molecule interacting atom***	***symmetry related molecule interacting atom***	***distance (Å)***
x-1, y, z	Arg82 Nη1	Ser112 O	3.24
	Arg82 Nη2	Asp113 Oδ1	3.22
	Ile126 N	Pro115 O	3.06
	Lys63 Nζ	Tyr116 O	2.84
	Lys63 Nζ	Pro115 O	3.13
	Gln98 Oε1	Tyr116 Oη	2.43
	Gly86 N	Met0 O	2.97
x, y-1, z	Gln71 Oε1	Gln35 Oε1	3.40
	Gln71 Nε2	Tyr88 Oη	2.99
x-½, -y-½, -z	Tyr99 N	Ser19 Oγ	2.92
	Ser19 Oγ	Gln49 Nε2	2.67
-x, y-½, -z-½	Arg65 Nη2	Leu5 O	2.53

Table S3: Atomic interactions between sulphate anions, glycerol and RNase 6 residues. Potential hydrogen bond distances have been considered using a cut-off distance of 3.4 Å.

ligand interaction site and atom		***interacting protein atom***	***distance (Å)***
S1	O1	HOH60	2.59
		HOH99	3.12
		HOH124	3.34
	O2	His122 Nδ1	2.66
		HOH42	3.02
		HOH81	2.70
	O3	Gln14 Nε2	3.22
		His15 Nε2	3.35
		HOH109	2.54
	O4	Leu123 N	2.79
		His15 Nε2	2.92
		HOH42	3.12
S2	O1	His67 N	3.21
		HOH70	3.11
		HOH98	2.67
		HOH118	3.32
	O2	HOH48	2.22
		HOH98	2.75
	O3	His67 N	3.20
		Arg66 Nε	2.64
		HOH98	2.62
S3	O1	*Arg92 Nε*	3.25
		Arg92 Nη2	3.05
		HOH82	3.02
	O2	*Arg92 Nε*	3.03
		HOH35	3.11
		HOH56	3.39
		HOH72	2.70
	O3	*HOH56*	3.26
	O4	Arg25 Nη1	2.33
		HOH52	3.14
S4	O1	His36 Nδ2	2.54
		B/HOH92	3.26
		HOH54	2.84
		Arg66 Nη2	3.39
	O2	HOH107	2.70
	O3	His39 Nε2	3.10
		B/HOH92	2.20
	O4	A/HOH92	3.15
		B/HOH92	3.21
GOL	O1	Ser 59 N	3.22
		HOH108	2.16
	O2	A/Ser59 Oγ	2.83
		HOH101	3.05
	O3	HOH36	3.29
		Gln110 Oε1	3.16

Table S4. Relative catalytic activity efficiency of RNase 6 in relation to RNase A.

	UpA	UpG	CpA	C>p	Poly(C)	Poly(U)	Poly(U):Poly(A)
RNase A	100	100	100	100	100	100	100
RNase 6	0.13	ND	0.02	0.07	0.41	3.25	26
RNase 3	0.01	ND	0.007	0.05	0.48	2.29	ND

Data are expressed in relative percentage values(%).
ND: Not detected at the assayed concentrations.

Table S5: Proposed RNase 6 residues involved in base and phosphate substrate subsite. Binding sites are labelled as defined for RNase A, where B_1 and p_1 are located at the main active site. Residues at hydrogen bond or van der Waals distances identified in the protein -heptanucleotide complex predicted by molecular dynamics are included.

Protein subsite	**Protein residue**
p_{-3}/p_{-2}	His36, His39, Lys87
B_{-2}	His36
p_{-1}	Arg82
p_0	Lys63
B_1	Thr42, Gln40
p_1	His15,Gln14, Lys38, His122
B_2	Asn64, Asn68, Arg66, His122
p_2	Lys7, Trp10

Table S6. Estimated pK_a values for selected His residues in RNase 6 and RNase A structures. Values were calculated using *ROSIE* (http://rosie.rosettacommons.org/ [2]).

	Residue	pK_a [a]
RNase 6[b]	His15	5.3
	His122	6.6
	His36	6.5
	His39	6.3
	His67 [e]	6.1
RNase A[c]	His12	5.8
	His119	6.8
	His105[e]	6.4
RNase A-K7H/R10H[d]	H7	6.8
	H10	6.7
	H12	5.8
	H119	6.4
	H105 [e]	6.5

[a] Starting reference pK_a values for His side chain pK_a was 6.3.
[b] Values calculated using RNase 6 crystal structure (PDB ID: 4X09).
[c] Values calculated using RNase A crystal structure (PDB ID: 7RSA).
[d] Values for RNase A-K7H/R10H crystal structure are taken from PDB ID:5ET4 (Blanco et al., unpublished results). Values are the average from the 4 protein chains at the asymmetric unit.
[e] His67(RNase 6) and His105 (RNase A) were taken as reference controls as solvent exposed His residue not involved in Coulombic interactions with neighbouring residues.

Figure legends

Figure S1: **A-D)** Electron density map for S1 to S4 sulfate anions and their respective protein environment residues. Water molecules are depicted with red crosses. Sigma 2Fo-Fc and FoFc electron density maps contoured at 1.5 and 3 sigma levels are shown (colored in dark and light blue respectively). Fo-Fc electron density map was built in the absence of ligands. Sulfate nomenclature corresponds to Table S3 numbering.

Figure S2. Catalytic activities were determined by the zymogram technique in 15% SDS-PAGE containing poly(C) as a substrate. **A.** (Lane 1) 750 pg of RNase A. (Lane 2) 120 ng of RNase 3. (Lane 3) 120 ng of RNase 6. (Lane 4) 120 ng of RNase 7. **B.** (Lane 1) 100 ng of RNase 6. (Lane 2) 100 ng of RNase 6 H15A-H36A. (Lane 3) 250 ng of RNase 6 H15A-H36A. (Lane 4) 500 ng of RNase 6 H15A-H36A. (Lane 5) 100 ng of RNase 6 H15A.

Figure S3. Structural superposition of RNase 6 and representative RNase A family structures (RNase A, RNase 1 and RNase 3). A) Overall structural superposition showing Loop L3. B) Amplification of L3 loop showing equivalent residues to His 36 and His 39 in RNase 6. RNase 6 is coloured in green, RNase A in blue, RNase 1 in magenta and RNase 3 in yellow. Picture was drawn with *PyMol 1.7.2* (Delano Scientific).

Figure S4. Poly(C) cleavage patterns by RNase 6-H15A and RNase 7-H15A. Both chromatograms correspond to the polynucleotide digestion products obtained after 30 min of incubation with 1.4 μM of enzyme.

References

1 Krissinel, E. and Henrick, K. (2007) Inference of macromolecular assemblies from crystalline state. J. Mol. Biol., England **372**, 774–797.

2 Kilambi, K. P. and Gray, J. J. (2012) Rapid calculation of protein pKa values using Rosetta. Biophys. J., United States **103**, 587–595.

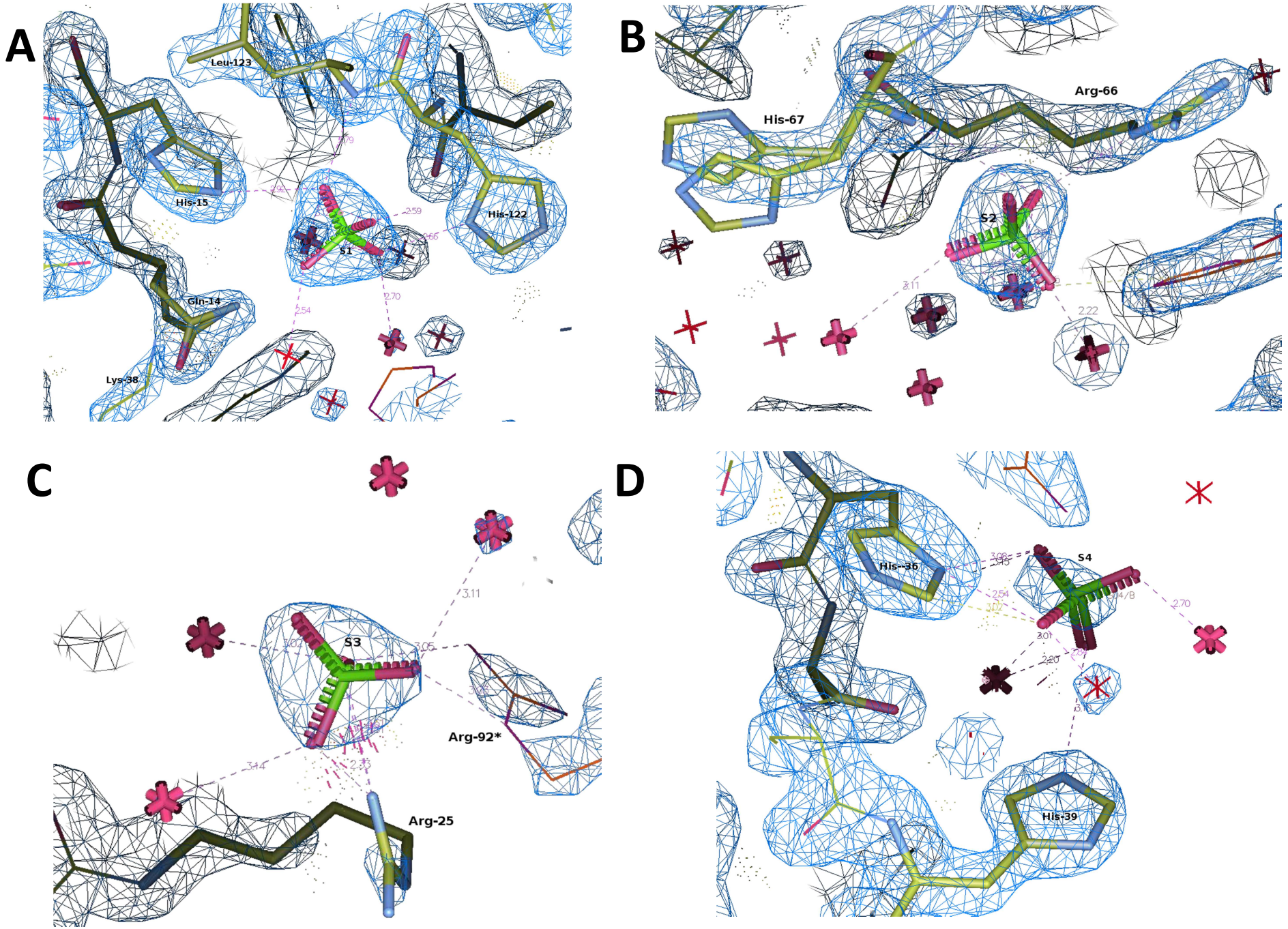
A
Leu-123
His-15
His-122
S1
Gln-14
Lys-38
B
Arg-66
His-67
S2
C
S3
Arg-92*
Arg-25
D
His--36
S4
His-39

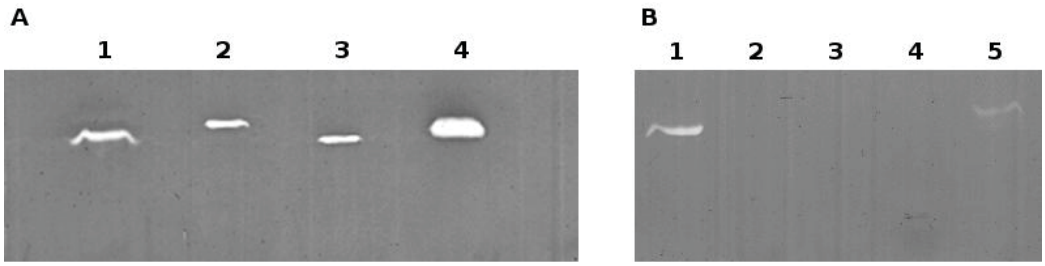
A
1
2
3
4
B
1
2
3
4
5

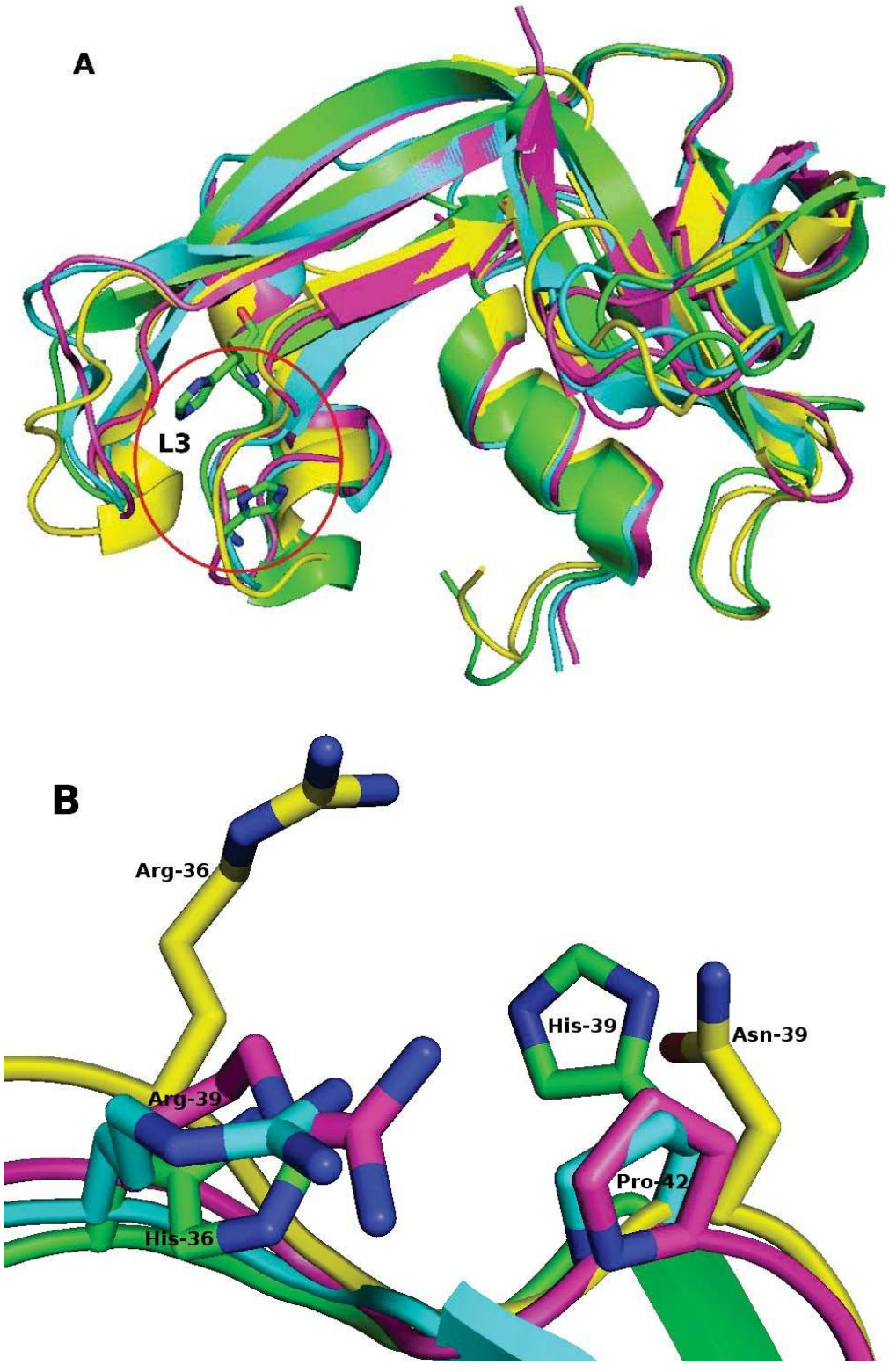
A
L3
B
Arg-36
Arg-39
His-36
His-39
Asn-39
Pro-42

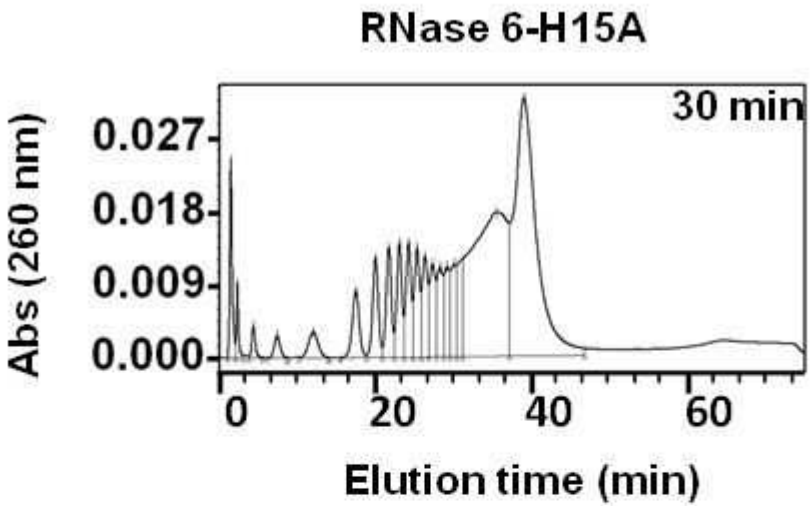
RNase 6-H15A
30 min
Abs (260 nm)
0.027
0.018
0.009
0.000
0
20
40
60
Elution time (min)

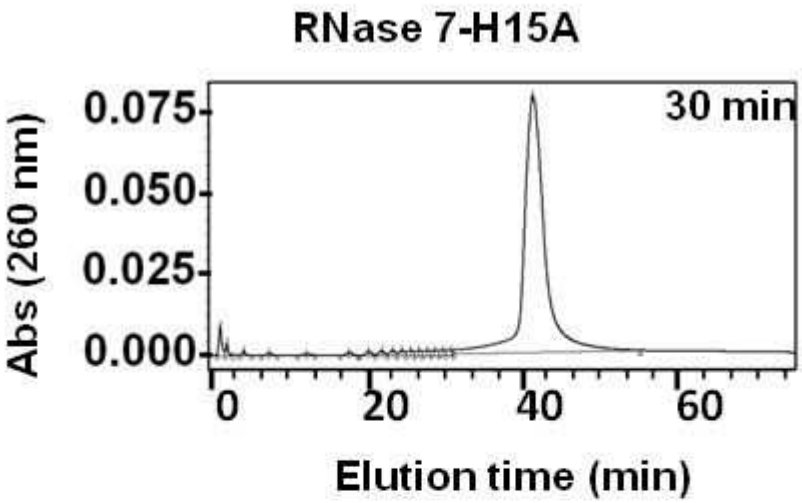
RNase 7-H15A
30 min
Abs (260 nm)
0.075
0.050
0.025
0.000
0
20
40
60
Elution time (min)